Heart-targeted Amelioration of Sepsis-induced Myocardial Dysfunction by Microenvironment Responsive Nitric Oxide Nanogenerators in Situ

Minzhi Ouyang

Second Xiangya Hospital, Central South University

Xiangnan Ouyang

Second Xiangya Hospital, Central South University

Zefang Peng

Hunan Provincial People's Hospital, The first affliated of Hunan Normal University

Minghui Liu

Second Xiangya Hospital, Central South University

Ganqiong Xu

Second Xiangya Hospital, Central South University

Zhen Zou

College of Chemistry and Chemical Engineering, Hunan Normal University

Ming Zhang (✉ zm7626@csu.edu.cn)

Second Xiangya Hospital, Central South University

Quanliang Shang

Second Xiangya Hospital, Central South University

Additional Declarations: No competing interests reported.

Abstract

Background: Reduced levels of bioavailable nitric oxide (NO) plays a key role in maintaining cardiovascular homeostasis. However, it is clinically proven that the lack of spatial and temporal control of release restrict the application of NO.

Destination: The purpose of this study is to design the heart-targeted and infection microenvironment-responsive NO-releasing biomaterials to efficiently ameliorate lipopolysaccharide (LPS)-induced cardiac dysfunction.

Methods and Results: The heart-targeted NO delivery and in situ release system was synthesized using hollow mesoporous silica (MSN) as the carrier and L-arginine (LA) as the NO donor. PCM-MSN@LA was characterized by several analytical techniques. The directed myocardial delivery was successfully accomplished by primary cardiomyocyte-specific peptide (PCM) targeting and low-intensity focused ultrasound (LIFU) guidance. Upon the LIFU irradiation, although the concentrations of LA released from PCM-MSN@LA was low, the research exhibited high sensitivity to the increased nitric oxide synthase (NOS) activity in the infection microenvironment. Rapid targeting of the heart and in situ NO release enabled PCM-MSN@LA in combined with LIFU exerted extraordinary protective effects against LPS-challenged myocardial injury by reducing the recruitment of inflammatory cells, inhibiting oxidative stress and maintaining the mitochondria integrity. In particular, PCM-MSN@LA+LIFU relieved but not aggravated the circulation collapse in the infection environment.

Conclusion: PCM-MSN@LA+LIFU exhibited significant cardioprotective effects against severe sepsis found in the hearts of the tested mice and reduced the side effects of NO diffusion. This technique could possibly be served as a new therapeutic method for sepsis-induced myocardial injury.

Background

Sepsis accounts for nearly 48.9 million deaths annually worldwide (1, 2). In the recent years, the COVID-19 pandemic that caused more than 1 million deaths has been recognized as the public health emergency of global concern (3). Septic cardiomyopathy is a leading type of sepsis-associated organ injury and plays the central role in increasing mortality; for instance, in patients who develop heart failure in sepsis, mortality exceeds 70%-90% (4-6). The mechanism of septic cardiomyopathy includes a dysregulated inflammatory response, oxidative stress and mitochondrial damage (7). Although advances in understanding the mechanism have been achieved, drug-resistant bacterial mutants and the complicated pathophysiology of septic cardiomyopathy hamper clinical outcomes. Reprogramming of the septic heart microenvironment is becoming a particular important supporting treatment for relieving heart failure by maintaining cardiac homeostasis in the context of sepsis.

Nitric oxide (NO) is an important signaling molecule in cardiovascular disease. NO donors were successfully ameliorated the injured myocardial microenvironment by inhibiting inflammatory cell recruitment, preventing excessive oxidant responses and stabilizing mitochondrial homeostasis (8-10).

According to the following reaction ($O_2^- + NO \rightarrow ONOO^-$), elevated reactive oxygen species (ROS) in sepsis consumes NO, consequently negates the NO bioavailability and promotes the tissue dysfunction (11, 12). Thus, increasing NO content in the early stage of sepsis maintains NO activity and further reduces ROS production without producing excessive peroxynitrite ($ONOO^-$). However, the delivery and manipulation of NO to the myocardium is still challenging, as the random diffusion and reactive chemical nature of NO in the circulation. Besides, the long-term taking organic nitrates leads to cyanide accumulation in the body (13). As an alternative NO donor, NO-donating nanoparticles attracted attention due to the stability in the circulation and can be modified by a variety of substances. To ensure the therapeutic NO on the septic myocardium, the nanoparticles should precisely target to the myocardium and followed by stimuli-responsive NO release.

MSNs were used in this study to enhance the stability of the NO donor. Attaching specific targeting moieties such as peptides to the surface of MSN@LA nanoparticles provides them with robust targeted delivery abilities (14). PCM, a phage display-isolated 20-mer peptide (WLSEAGPVVTVRALRGTGSW), binds cardiomyocytes 180 times more than control phage and exhibits specificity to cardiomyocytes, as shown by a 150-fold increase in fluorescence intensity for PCM on floating PCM cells than on other cell types such as myoblasts and hepa1-6 cells (15). To further improve myocardial-targeting, therapeutic ultrasound has been recommended as an efficient technique for targeted delivery, and this technique is also known as low-intensity focused ultrasound (LIFU) (16, 17). When exposed to LIFU irradiation, bioactive agents are carried to specific tissues due to transient increases in cell membrane permeability by bursting microbubbles (18, 19). Therapeutic ultrasound usually has a frequency range of 0.75-3 Hz, and 1-2 Hz is most frequently used (19). This dual targeting system including PCM targeting and LIFU irradiation could precisely transfer LA to the myocardium.

Various of polymer- and lipid-encapsulated NO donor delivery carriers have shown some benefits in prompting vasodilation in stroke (20), restoring glucose homeostasis (21) or fighting cancer (22, 23), no records related to septic cardiomyopathy cure. As we known, the NO in living cells was mainly synthesized by nitric oxide synthases (NOSs) from L-arginine. There are three isoforms of the enzyme: constitutively expressed endothelial (eNOS) and neuronal (nNOS) isoforms and the inducible isoform (iNOS) (24). Under sepsis condition, the infected environment exhibits different characteristics from normal condition, one of them was NOSs expression elevation. In the early phase of sepsis, the iNOS and eNOS increased nearly 2-3 times (25). Based on the performance, it is expected that LA, a natural NO donor with excellent biocompatibility, can liberate NO in the presence of NOS-rich septic microenvironment. Therefore, we believe that NO-donating nanoparticles can play the role of NO in cardiovascular protection responded to sepsis microenvironment change.

Finally, we successfully synthesized a myocardium-targeted nanoscale carrier system that could generate NO in the heart without causing nitrate/nitrite accumulation in the circulation. In the early phase of sepsis, this targeted gas therapy efficiently improve the myocardial function by resulting in the of inflammatory response alleviation, ROS production reductions, myocardial mitochondria protection. This strategy might

be applied as a timely treatment to ameliorate the septic microenvironment and assist the antibiotics appliance, paving way for the cardioprotective effects.

Methods

1. Synthesis of PCM-MSN@LA

3-aminopropyltrietho xysilane (APTS), N-Cetyltrimethylammonium bromide (CTAB, 99%), N-hydroxysuccinimide (NHS, 98%) and 1-ethyl-3-(3-dimethylaminopropyl) carbodiimide (EDC, > 97%) were purchased from Alfa Aesar (Tianjing, China). HCl solution (37%) and sodium hydroxide (NaOH) were obtained from Xilong reagent company (Guangdong, China). The FITC-labeled PCM and FITC-labeled scramble peptide ligand were synthesized by Sangon Biotech Co., Ltd (Shanghai, China). The sequence of PCM was DPVWEYPLEFSWDTGWGDSS. The sequence of scramble peptide was random selected as WLSEAGPVVTVRALRGTGSW, keeping the same fragments with PCM.

CTAB (1.00 g, 2.74 mmol) and NaOH solution (3.5 mL, 2.00 M) were dissolved in 520 mL of deionized water and heated to 80°C. Next, 5.0 mL TEOS solution was slowly dropped to the solution. The mixture solution was stirred at 80°C for 2 h. Within 10 min in the 8700 g speed for centrifugation, the crude product was sequentially isolated. The collections were washed thoroughly with water and ethanol for times. To remove the CTAB, the sample (0.7 g) was dissolved in a mixture of ethanol (70 mL) and concentrated HCl (0.70 mL, 37.2%). Sixteen hours later, the organic solvent was washed using deionized water at least 3 times to obtain MSN. MSN (1 g) was dissolved in 100 ml of anhydrous toluene via sonication. APTS (1 mL) was added and reacted for 20 hours. White particles were collected through centrifugation and sequentially washed three times with ethyl alcohol and three times with deionized water. Then 0.8 ml of HCl was added and the flask was heated at 80 °C for 16 h to dislodge CTAB, we obtained MSN-NH$_2$ sediment. MSN-NH$_2$ nanoparticles were dried via lyophilization.

Then, 100 mg of MSN-NH$_2$ was dispersed in 20 ml of PBS buffer, 0.03 mg of N-hydroxysuccinimide (NHS) and 0.3 mg of a 1-ethyl-3-(3-dimethylaminopropyl) carbodiimide (EDC) mixture was added into the solution at room temperature and stirred overnight. PEG molecules were added and reacted for 12 h to generate PEG-MSN-NH$_2$ via an amidation reaction. FITC-labeled scramble peptide or FITC-labeled PCM was dissolved in DMSO buffer and then incubated with PEG-MSN-NH$_2$ for 28 h. The residue was extracted by centrifugation three times and dried via the lyophilization method.

PCM-MSNs (20 mg) were dispersed in 10 ml of saturated LA solution and mixed without light irradiation for 20 h. After centrifugation (8700 g, 5 min) for five times, the products were washed three times and vacuumed drying to acquire the final PCM-MSN@LA nanoparticles.

A total of 1 mg of PCM-MSN@LA was diluted with 1 ml of PBS and stored at 4 °C before incubation or injection.

2. Characterization of PCM-MSN@LA

PCM-MSN@LA nanoparticles were prepared for size, zeta, FTIR and morphology assessments via DLS (Malven Zetasizer, Nano ZS90), an infrared spectrometer (Nicolet, Avatar360) and transmission electron microscopy (TEM, FEI, TecnaiG2F20). Additionally, a thermal gravimetric analyzer (Setaram, S60/51920) was used to ensure peptide conjugation and LA encapsulation. The mean particle size and zeta were measured using DLS from day 0 to 28 to evaluate the stability of nanoparticles.

3. L-arginine loading and L-arginine release using LIFU in vitro

Unlabeled PCM was used for the assessment.

Five milliliters of PCM-MSN@LA was placed in a dialysis bag (molecular weight cutoff = 3500), and the dialysis bag was placed in an opaque centrifuge tube containing 20 mL of pH 7.35-7.45 or pH 7.0-7.3 HEPES buffer (50 mM HEPES, 2 mM $CaCl_2$). Then, the centrifuge tube was gently shaken at 200 rpm min^{-1} at 37 °C. At 36 min intervals for 10 h, 100 µl of the buffer solution was withdrawn and mixed with a 10% ninhydrin solution. The intensity of the LA characteristic peak at 570 nm was recorded via an ultraviolet spectrophotometer (Shimadzu, UV2700). For ultrasound-triggered LA release, LIFU (1.0 W/cm^2-20% power-10 s per cycle, 10 cycles, 10 s intervals) was simultaneously performed on the bottom of the tube using a Sonitron 2000 V (Vepa Gene, Co., Ltd., Chiba, Japan). The absorbance intensities were recorded.

The loading and release profiles of LA were acquired according to a standard curve as a function of the mass concentration of LA molecules.

4. Isolated primary cardiomyocytes culture and animal feeding

All animal experiments were performed with the approval of the Institutional Animal Care and Use Committee of Central South University (Changsha, China).

Neonate cardiomyocytes from 1-day-old C57/BL6 mice were purchased from Hunan SJA Laboratory Animal Co., Ltd. (Hunan, China). Firstly, the heart was enzymatically digested with 2.5 mg mL^{-1} trypsin Aladdin Co., Ltd, Shanghai, China , and then perfused with digestion buffer containing 2 mg mL^{-1} DNase I (Sigma, D7291). Finally, the tissue pieces were centrifuged for cardiomyocyte collection. These isolated cardiomyocytes were cultured on 20% FBS (Biological Industries, 04-001-1ACS), 40 IU ml^{-1} penicillin (Sigma, P3032), 1.6 µg ml^{-1} VitB12 (Sigma, V6629) and 0.1 mmol L^{-1} 5 -bromo-2 -deoxyuridine (Sigma, B5002) in DMEM (HyClone, C11995500BT) under normal conditions (5% CO_2, 21% O_2 and 74% N_2).

Male C57/BL6 mice were purchased from Hunan SJA Laboratory Animal Co., Ltd. (Hunan, China), housed and maintained at room-temperature in an air-conditioned environment. They were 8–12 week-old, male and weighed between 20–30 g.

5. The safety of PCM-MSN@LA

The change in particle size and zeta from day 0 to 28 was observed using DLS.

Cell Counting Kit 8 (CCK-8): Cardiomyocytes were seeded in 96-well plates at a density of 1×10^4 per well and cultured for 24 h. Various concentrations (0.05 mg ml^{-1}, 0.1 mg ml^{-1}, 0.2 mg ml^{-1}, 0.4 mg ml^{-1}, 0.6 mg ml^{-1}, 0.8 mg ml^{-1}, and 1 mg ml^{-1}) of PCM-MSN@LA were loaded into the cardiomyocytes. After incubating for 24 h, the cells were collected and stained with a CCK-8 proliferation kit (Dojindo, CK04), and the absorbance was measured at 450 nm.

Hematoxylin-eosin (HE) staining: Twenty-four hours after injection with 50 mg kg^{-1} PCM-MSN@LA, the major organs, including the lung, liver, spleen, kidney and heart, were isolated and washed with normal saline 3-5 times until the blood was cleared. Then, some of the organs were fixed in 10% buffered formalin and embedded in paraffin. Paraffin sections (≤5 µm) were stained with hematoxylin and eosin (HE) at 37 °C for 15 min. The slides were observed under a light microscope (Carl Zeiss AG, Oberkochen, Germany) at a magnification of 40×10.

6. Evaluation of cell uptake and biodistribution in the myocardium of the targeted NO release system

To prepare the nanoparticles for biodistribution evaluation, a few drops of Cy5.5 fluorescent dye was added to replace L-arginine loading. The FITC-stained PCM and scramble peptide were changed to unstained PCM and scramble peptide as well.

Groups: To demonstrate the ability of PCM to bind to cardiomyocytes, three treatments were carried out: scramble peptide MSNs or PCM-MSNs with cardiomyocytes and PCM-MSNs with HepG2 cells.

Cell colocalization staining: Both cardiomyocytes and HepG2 were seeded in 6-well plates at a density of 1×10^4 per well. The cardiomyocytes were incubated with fresh DMEM containing 50 µg ml^{-1} PCM-MSN and scramble peptide MSNs separately for 1 h. The HepG2 were incubated with the same concentration PCM-MSN. After discarding the culture media, the cells were washed with PBS (pH 7.4) three times. Then, 4% paraformaldehyde was used to fix the cells at room temperature, and 0.1% Triton X-100 was simultaneously added to the cells for 10 min for permeabilization. All cells were double stained. The cells were perfused with R-PE stained anti-sarcomeric alpha actinin (α-SA) (Abcam 137346 1:100) at 4 °C overnight at room temperature which was used to specific labeled cardiomyocyte (17). After being washed with PBS, the cells were counterstained in a 4 6-diamidino-2-phenylindole (DAPI) (Sigma, D9542)

solution for 15 min to label the nucleus. Cardiomyocyte internalization was assessed using a confocal laser scanning microscope (CLSM, Olympus FluoView FV3000). The fluorescence intensity was graphed according to the white line of merged fluorescence images.

Fluorescence images in vivo: Mice were divided into 3 groups for myocardial binding efficiency assessment: MSN, PCM-MSN, and PCM-MSN+LIFU (4 mice in each group). After anesthetization with 1% pentobarbital (50 mg kg^{-1}), each type of nanoparticle vesicle was injected via the tail vein at a dose of 50 mg kg^{-1} body weight. The transducers were placed at the heart 1 min later. Ultrasound was transmitted at 1.0 W/cm^2-20% duty power for 10 s per cycle, 10 cycles, 10 s intervals. Six hours later, the organs, including the heart, lung, spleen, liver and kidney, were isolated and washed with PBS for several times to wash away the blood. Florescence signal distribution was visualized with in vivo images (PerkinElmer, IVIS lumina III). Heart cryosections (2 mm thickness) were prepared to further observe cardiac localization. Quantitative analysis was performed using Living Image 5.0 software.

7. Intracellular NO release

Cardiomyocytes were seeded in a 6-well cell culture plate at a density of 1×10^6 per well and then cultured with 10% FBS and 1% penicillin/streptomycin. A sepsis model was established by incubating the cells with 1 μg ml^{-1} LPS (Sigma, *Escherichia coli*, O111:B4).

After the cells were incubated for 24 h, PCM-MSN@LA (25 μg ml^{-1}, 50 μg ml^{-1}) were added to control group (untreated cardiomyocytes) and PCM-MSN@LA (25 μg ml^{-1}, 50 μg ml^{-1}, 75 μg ml^{-1}, 100 μg ml^{-1}) were added to LPS-treated cardiomyocytes. Two hours later, a milliliter of supernatant was removed for nitrite level assays with a Griess assay kit (Beyotime Biotechnology, S0021, Haimen, China) using an ultraviolet spectrophotometer (Shimadzu, UV2700, Japan). To analyze NO generation in LPS-treated cardiomyocytes over time, 75 μg ml^{-1} PCM-MSN@LA was incubated with cardiomyocytes, then LIFU (1.0 W/cm^2-20% duty power-10 s per cycle-10 cycles) was carried out at the bottom of the plate. At different time points (pre, 5 min; 15 min; 30 min; 2 hours; 6hours), the NO fluorescent probe DAF-FM DA (Beyotime Biotechnology, S0019) was incubated with the cells for 20 min at 37 °C in darkness. And the unloaded probe was removed by three washes with PBS. The variations in nitrite levels in cardiomyocytes were quantitatively monitored by CLSM (Olympus FluoView FV3000). The fluorescence intensity was quantified.

8. Cardiomyocytes viability and superoxide assessment.

Cardiomyocytes were invided into 5 groups. They were named control (cells without any threatment), LPS (cells incubated with LPS), PCM-MSN (PCM-MSN was added to the cells simultaneously with LPS), PCM-MSN@LA (PCM-MSN@LA was added to the cells simultaneously with LPS), PCM-MSN@LA+LIFU (PCM-MSN@LA was added to the cells simultaneously with LPS, the LIFU was irradiated on the bottom of the

plate) separately. The concentration of LPS was 5 μg ml^{-1} and thelevel of PCM-MSN@LA used was 75 μg ml^{-1}. Ultrasound was performed using the following parameters: 1.0 W/cm^2-20% duty power-10 s per cycle-10 cycles with a 10 s interval between two cycles in total. After 6 hours, the cells were stained with a CCK-8 proliferation kit as mentioned before. The absorbance was measured at 450 nm. Additionally, cardiomyocytes were seeded in special 35mm-size, 0.17 mm-thick dishes (Nest, N801001) at a density of 1×10^4 cells per well and cultured for 24 h. Six hours after the different treatments were performed, the cells underwent TUNEL staining (Beyotime Biotechnology, C1091) and DCFH-DA staining (Beyotime Biotechnology, S0033) respectively. The cells were washed three times and examined by laser confocal microscopy. The number of positive cells was calculated by Image-Pro Plus software version 6.0 (Media Cybernetics, Bethesda, MD).

9. Myocardium-targeted NO production in vivo

Animal treatment: An endotoxic shock model was established as following. Lipopolysaccharide was dissolved in bacteria-free PBS and diluted to a final concentration of 5 mg ml^{-1} for intraperitoneal injection. The C57/BL6 mice were anesthetized using pentobarbital sodium (50 mg kg^{-1}), and administered by 0.5mL of PBS or 0.5ml of PBS with LPS (10 mg kg^{-1} body weight) via intraperitoneal injection. Immediately, 1 mL of saline was injected subcutaneously at 37 °C for fluid resuscitation.

To verify the treatment efficacy, 48 mice were randomly divided into six groups:

(1) Control (mice administered 1 mL of prewarmed normal saline);

(2) LPS (LPS-injected mice);

(3) PCM-MSN (1 mg kg^{-1} PCM-MSN injected 2 min after LPS);

(4) MSN@LA (1 mg kg^{-1} MSN@LA injected 2 min after LPS);

(5) PCM-MSN@LA (1 mg kg^{-1} PCM-MSN@LA injected 2 min after LPS);

(6) PCM-MSN@LA+LIFU (1 mg kg^{-1} PCM-MSN@LA injected 2 min after LPS, and LIFU was applied 1 min later).

The LIFU parameters were 1.0 W/cm^2-20% duty power-10 s per cycle-10 cycles with 10 s intervals. Another 36 mice were divided into the same six groups to examine the survival rates.

Measurement of blood markers, including LDH, CK-MB and cTnI, was performed. Blood samples were collected from the inferior vena cava 6 h after LPS injection and centrifuged at 589 g min^{-1} for 10 min at 4 °C for analysis. Plasma concentrations of LDH and CK-MB were measured using an automatic biochemical analyzer (Hitachi, 7600), and the level of cTnI was measured by an Quantikine mouse ELISA kit (Cusabio, CSB-E08421).

Measurement of blood pressure: Systolic blood pressure (SBP) and diastolic blood pressure (DBP) were monitored using P-600A automatic noninvasive blood pressure measurement system (TECHMAN, Chengdu, China). Following different treatments 6 hours, the mice were placed the receiver pad adjacent to the tail-cuff device and synchronizing instrument clocks. The data were recorded throughout the duration of each noninvasive measurement session.

Echocardiography: Echocardiography was performed at 6 h after CLP under light anesthesia with 2% isoflurane inhalation via an isoflurane delivery system. All images were obtained from an ultrasound scanner (FujiFilm Visual Sonics Vevo 2100) coupled with a 30.0-MHz linear transducer. Left ventricular (LV) diameters at end diastole and end systole (LVEDD/LVESD) were measured from M-mode images in the short axis view at the papillary muscle level. LV systolic function-fraction shortening (FS) and ejection fraction (EF) were calculated using Visual Sonics Measurement Software. Left volumes at end diastole and end systole (LV VOL d/LV VOL s) were evaluated using improved Simpson's method by tracing the endocardium manually on apical two chamber view at end diastole and end systole tracing from 3 cardiac cycles.

Histopathological assessment: After 6 h after LPS injection, hearts were fixed in 4% paraformaldehyde (PH 7.4). Following paraffin embedded, the tissues were cut into 5-μm-thick sections for HE staining which mentioned above.

Electron microscopy assay: Hearts were cut into multiple 1 mm fragments and fixed in 2.5% glutaraldehyde. The tissues were rinsed with PBS and then fixed in 1% osmium tetroxide (OsO4; Sinopharm Chemical Reagents Co., Ltd., Shanghai, China) in 0.1 M PBS for 1 h at room temperature. The sections were for transmission electron microscopic examination (ZEISS 906, Germany).

Immunohistochemistry examination: To assess the cell apoptosis, hearts were isolated and placed in a 15% sucrose solution at 4 °C to prepare frozen slides (4-μm-thickness). Then, the heart slides were blocked with endogenous avidin (Leagene Biotechnology Co., Ltd., Beijing, China) at room temperature for 20 min, then the samples were stained with TUNEL staining in accordance with the manufacturer's instructions (KeyGEN BioTECH Co., Ltd., Jingsu, China). Besides, the different immune cells were stained using antibodies and dilutions: anti-rat Ly-6G antibody (Abcam, ab25377, 1:50) and goat anti-rat IgG secondary antibody (Life Technologies GmbH, Darmstadt, A10517, 1:200). Sections were washed 5 times and developed with a 3,3'-diaminobenzidine kit (DAB). All slides were counterstained with hematoxylin and observed by light microscopy (NIKON ECLIPSE C1, Japan).

Immunofluorescence staining: Hearts were sliced into sections for staining. Cellular reactive oxygen species were measured by dihydroethidium (DHE) labeling according to the manufacturer's instructions. DHE (Sigma, D7008) was added to the marked area and then incubated at 37 °C for 30 min in darkness. Following, slides were stained with DAPI for 5 min and washed to prepared for coverslips. The images were taken by fluorescence microscopy (Nikon Eclipse C1, Nikon, Japan).

Malondialdehyde (MDA) measurement: MDA is a stable metabolite of lipid peroxidation products. Heart samples were dissolved in 60 ml of phosphate-buffered saline (pH 6). Tissue homogenate (0.1 ml) was mixed well with 0.2 ml MDA colorimetric activity assay kit reagents (Beyotime Biotechnology, S0131S). The mixture was incubated at 100 °C for 15 min in a water bath and then centrifuged for 10 min at room temperature. The rate of change in absorbance at 532 nm was recorded using a spectrophotometer (Cecil Instruments, Ltd., CE 9000, UK).

Western blot: Heart tissue homogenates were used for Western blot analysis. Proteins were separated using 10% or 12% SDS−PAGE and transferred to PVDF membranes, which were incubated with the following primary antibodies: iNOS (Abcam, 178945, 1:1000), eNOS (Abcam, 199956, 1:1000), NLRP3 (Adipogen, AG-20B-0014, 1:1000), NF-κB P65 (Cell Signaling Technology, 8242, 1:1000) and Cleaved-caspase3 (C-caspase3) (Cell Signaling Technology, 9964, 1:1000). After being washed, the membranes were incubated with HRP-conjugated secondary antibodies at room temperature for 1 h and developed via an ECL system (Amersham Biosciences, USA). Tubulin (Proteintech, 10094-1-AP, 1:5000), GAPDH (Proteintech, 10494-1-AP 1:10000) was used as an internal control.

Real-time PCR: Total RNA was collected from each sample and analyzed by real-time PCR. The levels of gene expression were determined using the comparative Ct method, and relative amounts were normalized to GAPDH mRNA. The oligonucleotide primers for IL-1β, IL-6, IL-18, TNF-α, and GAPDH are shown in Table 1.

Table 1. Primer sequences used in RT-qPCR experiments

Gene	Primer	Sequence
IL-1β	Forward	AAAAATGCCTCGTGCTGTCT
	Reverse	TCGTTGCTTGTCTCTCCTTG
IL-6	Forward	GGAGTTCCGTTTCTACCTGGA
	Reverse	TGGAAGTTGGGGTAGGAAGG
IL-18	Forward	TGACAAAAGAAACCCGCCTG
	Reverse	GGTCACAGCCAGTCCTCTTA
TNF-α	Forward	CGTCGTAGCAAACCACCAAG
	Reverse	AGCCTTGTCCCTTGAAGAGA
GAPDH	Forward	ACAGCAACAGGGTGGTGGAC
	Reverse	TTTGAGGGTGCAGCGAACTT

Statistical Analysis

All experiments were repeated three times and the data are presented as the mean ± standard error (SD). Comparisons among groups were performed with one-way ANOVA followed by Student's t test using GraphPad Prism 5.0 software. Survival rates were evaluated with the log-rank test. $*p < 0.05$ was considered significant and $**p < 0.01$ was very significant.

Results

1. Characterization of PCM-MSN@LA

PCM-MSN@LA was spherical in shape (Fig. 2a) with good dispersion (Fig. 2b). First, PCM was conjugated to MSNs, leading to increased diameters from 132.67 nm to 179.33 nm and decreased zeta potentials from − 19.17 mV to 3.52 mV. After loading LA, the diameter changed to 186.67 nm, and the surface charge changed to a negative position of -6.23 mV (Fig. 2c & d). The powder X-ray diffraction (XRD) pattern of the nanoparticles showed a hexagonal array that could be indexed as (100), (110), and (200) Bragg peaks (Fig. S1). In the N_2 adsorption-desorption measurements, the specific surface areas of MSN-NH_2, PCM-MSN and PCM-MSN@LA were 764.332 m² g^{-1}, 661.83 m² g^{-1} and 62.07 m² g^{-1}, respectively, indicating that some channels of mesoporous nanoparticles were occupied by PCM and filled with LA (Fig. 2e). Therefore, PCM and LA were successfully grafted to MSN nanoparticles. Beside, PCM and LA were accounted for nearly 39.7% and 20.2% of the weight of PCM-MSN@LA, respectively, as determined by TG analysis (Fig. S2). The in vitro stability of PCM-MSN@LA in saline is an important component in evaluating its physicochemical properties. As shown in Fig. 1f & g, PCM-MSN@LA maintained high stability, showing no notably change in size distribution and Zeta potential during 30 days of storage at 37°C in PBS (Fig. 2f & g).

2. LA encapsulation and release profiles of PCM-MSN@LA and the cytotoxicity assay.

According to the standard curve of LA absorption intensity measured by UV−vis (Fig. S3), the amount of LA calculated in 10 mg of PCM-MSN@LA was 2.4 mg. In addition, 11.5% or 16.9% of LA was released from PCM-MSN@LA within 520 min in HEPES buffers at pH 7.35−7.45 and pH 7.0-7.3, respectively. LIFU improved the LA release efficiency, and the release rate rose to nearly 25.6% (pH 7.35−7.45) and 35.3% (pH 7.0-7.3). (Fig. 3a & b). The CCK-8 assay showed no detectable cytotoxicity of PCM-MSN@LA to cardiomyocytes at concentrations below 1 mg ml^{-1} (Fig. 3c). In addition, histopathological images of major organs, including hearts, livers, spleens, lungs, and kidneys, of the treated mice showed minor change in tissue architecture in response to intravenous injection of 50 mg kg^{-1} PCM-MSN@LA compared to those of untreated mice (Fig. 3d). Furthermore, from the measurement of hemolysis to evaluate the toxicity of PCM-MSN@LA (Fig. 3e), no hemolysis was apparent after 3h blood incubation, even at high nanoparticle doses (i.e., 3200 mg mL^{-1}).

3. Cellular uptake of PCM-MSNs in vitro and assessment of PCM-MSN@LA + LIFU biodistribution in vivo.

The targeting of PCM to primary cardiomyocytes is shown in Fig. 3. As expected, PCM showed high affinity for cardiomyocytes, as confirmed by strong green fluorescent FITC-labeled PCM signals conjugated to red fluorescent PE-stained cardiomyocyte-specific marker (α-SA) signals in the PCM-MSN group (Fig. 4a). In contrast, the scramble peptide insufficiently targeted cardiomyocytes, as evidenced by weak green fluorescent FITC-labeled scramble peptide signals accumulating around cardiomyocytes (Fig. 4b). In addition, few PCM-MSNs adhered to HepG2 cells showed as considerably low internalization of FITC-labeled PCM in DAPI-stained HepG2 cells (Fig. 4c), meaning that PCM was specific for cardiomyocyte.

To assess the targeting capability of PCM and LIFU in vivo, red regions of Cy5.5 staining, which represented nanoparticles in major organs, were visualized. With PCM guidance, PCM-MSNs were efficiently transported to the heart, as evidenced by a nearly 60-fold higher red florescence intensity accumulation in the heart compared to that in the MSN group. Furthermore, when PCM-MSN and LIFU mixed, the mice heart exhibited 7-fold more red florescent intensity than that of the single PCM-MSN (Fig. 5a & b). Irradiated by LIFU to the heart enable PCM-MSNs more easily penetrate through cardiac microvessels and arrive at the myocardium. Additionally, the images of the major tissues, including hearts, livers, kidneys, lungs and spleens showed that evidently high localization of PCM-MSNs in cardiac tissues but not other organs, suggesting that double targeting with PCM and LIFU ensured the delivery of nanoparticles to the heart (Fig. 5c & d).

4. NO production from the myocardium-targeted NO release system in cardiomyocytes

NOS expression is required to generate NO from LA. Upon the invasion of LPS, the internal environment exhibited elevated NOS expression. As manifested by Fig. 6a, the iNOS and eNOS levels showed enhanced expression in cardiomyocytes from 30 min to 12 hours after LPS stimulation. Meanwhile, iNOS and eNOS expression peaked at 2 hours and 6 h, respectively (Fig. 6a & b).

The NO production capacity of PCM-MSN@LA in combination with LIFU in cardiomyocytes was further studied by measuring NO levels through Griess assays and florescence microscopy after DAF-FM DA staining. Without LPS treatment, neither 25 µg ml-1 nor 100 µg ml-1 PCM-MSN@LA released noticeably more NO than in untreated cells, proving that PCM-MSN@LA could effectively produce NO only in the context of infection. Increased nitrite levels were generated when the PCM-MSN@LA were incubated with LPS-treated cardiomyocytes. Besides, with the LPS infection, the augmented levels of nitrite were associated with the concentration of PCM-MSN@LA (Fig. 6c). The mean absolute nitrite level was 0.56 µM after 2 hours of LPS and PCM-MSN@LA stimulation, which was significantly increased compared with 0.5 µM after LPS stimulation only. Interestingly, although the significant difference was observed

before and after PCM-MSN@LA being incubated with LPS-treated cardiomyocytes, the NO concentration maintain low in cells. As we known, at low concentrations, NO controls circulating blood flow and white blood cells, which are important in cardiovascular homeostasis (24). Likewise, photomicrographs of DAF-FM DA stained NO production in LPS-induced cardiomyocytes showed that green fluorescence was enhanced from 5 min to 6h after 75μg ml-1 PCM-MSN@LA incubation in combined with LIFU, meaning that the PCM-MSN@LA + LIFU sustained releasing NO at least 6 hours (Fig. 6d).

5. The effect of PCM-MSN@LA on LPS-induced injury in cardiomyocytes

Cardiomyocyte apoptosis following LIFU-mediated PCM-MSN@LA delivery was evaluated by CCK-8 assays and TUNEL staining analysis. A massive cells damage was induced by LPS, whereas a modest damage was observed in cells treated with PCM-MSN@LA and PCM-MSN@LA + LIFU (cell viability was 62% vs. 72%, 80%) (Fig. 7a). It is also showed by TUNEL staining test, that LPS severely restricted the cardiomyocyte viability, manifested as quantities of TUNEL-stained positive cells present in LPS group. Treatment with PCM-MSN@LA but not PCM-MSN apparently decreased the percentage of apoptotic cells, let alone PCM-MSN@LA + LIFU. The PCM-MSN@LA + LIFU group achieved the fewest TUNEL-positive cells (Fig. 7b). To confirm the effect of LIFU-mediated PCM-MSN@LA on ROS scavenging, the intracellular ROS probe DCFH-DA was used. As shown in Figure. 7c, the average ROS level in cardiomyocytes that were treated with LPS decreased after incubated with PCM-MSN@LA with or without LIFU for 6 h. However, the level was not statistically changed after PCM-MSN incubation. This finding showed that ROS reduction was associated with NO release in cardiomyocytes.

6. Myocardium-targeted NO release inhibited cardiac apoptosis and raised survival rate in sepsis

The protective effect of targeted NO release on LPS-induced myocardial injury was first evaluated by TUNEL assays. Numerous necrotic cells labeled by brown fluorescence were noted in the cardiomyocytes after LPS administration. Conversely, those cells were effectively depressed by PCM-MSN@LA treatments, especially PCM-MSN@LA + LIFU (Fig. 8a & b). Similarly, there was no remarkable change in the apoptotic index protein cleaved caspase-3 expression in group (3) and group (4). By contrast, remarkable expression decreases were obtained in group (5) and group (6). The minimal expression achieved in group (6) (Fig. 8c & d). The fact suggests that a low concentration of LA affected the myocardium in sepsis if it could be delivered to the heart quickly. Finally, the protection of cardiac function was closely related to the survival rate. As expected, the survival rates were only significantly higher in both PCM-MSN@LA treatment groups, including group (5) and group (6). When PCM-MSN@LA was combined with LIFU, the lifespan prolonged well (Fig. 8e).

7. Localized NO release protected cardiovascular function from myocardial injury during sepsis

To verify whether myocardium-targeted NO release protected heart function from sepsis deterioration, serum markers, echocardiography, blood pressure viability and histological analysis were measured. Serum markers included cTnI, CK-MB and LDH. Mice injected with LPS exhibited 9-fold higher cTnI and CK-MB levels (3739.9 ± 182.3 vs. 430.4 ± 27.2; 2026.3 ± 370.2 vs. 253.9 ± 57.6), and 6-fold higher LDH levels (1344.4 ± 240.5 vs. 259.9 ± 50.5) than controls. There was a slight variation of those markers between mice injected with PCM-MSN or MSN@LA after LPS injection and mice injected with LPS only. Instead, the mice injected with PCM-MSN@LA, especially irradiated by LIFU presented apparently drop. The reduction rates were 37%, 31% and 21% in group (5) and 53%, 47% and 39% in group (6) (Fig. 9a-c). Then, echocardiography analysis showed that 6 h after LPS injection, the two PCM-MSN@LA-treated groups showed significantly higher EF and FS as well as lower LV VOLs and LVIDs than the LPS group. Though not statistically different, group (6) still presented better performance than group (5). There were nearly no differences in any echocardiographic parameters among group (3), group (4) and group (2) (Fig. 9d). The M-mode in the short-axis view was showed in Fig. 9e. Similarly, from H&E staining assays, edema, inflammatory cell infiltration accompanied by disorganized myocardial fibers was present in the LPS group (Fig. 9f). However, the PCM-MSN@LA and PCM-MSN@LA + LIFU treatments reduced the degree of edema and fibrosis in cardiac suggesting that LA transfer to NO, followed by precisely located to the heart tissue, resulting in cardiac function prevention in sepsis. Hypotension is another major hemodynamic disorder that is closely linked to mortality in sepsis. All septic mice exhibited lower blood pressure than controls despite fluid resuscitation. PCM-MSN treatment did not change the hypotension. Worse, MSN@LA treatment aggravated blood pressure disorder. Unlikely and surprisingly, PCM-MSN@LA treatment, especially that mediated by LIFU, significantly mitigated the LPS-induced hypotension (Fig. 9g). Accordingly, the PCM-MSN@LA + LIFU therapy was associated with cardiovascular deterioration reverse in sepsis without side effect of promoting vasodilatation. Thus, the elaborately designed PCM-MSN@LA can be integrated in LIFU irradiation for efficiently alleviating myocardial dysfunction in sepsis.

8. The mechanic of myocardium-targeted NO release on LPS-induced cardiac dysfunction

The outstanding myocardium protection effect of PCM-MSN@LA + LIFU in vivo during sepsis can be attributed to the following three reasons: (1) regulating the myocardial inflammatory response; (2) ameliorating oxidant stress; (3) maintaining mitochondrial function.

The general consequences of LPS included overwhelming inflammatory cytokine accumulation (Fig. 10a-d) and a large quantity of inflammatory-associated protein expression (Fig. 10e & f). Delivery of PCM-MSN@LA, especially irradiated by LIFU, significantly regressed the excessive inflammatory response as evidenced by the statistically reduction of cardiac IL-1β, IL-6, IL-18 and TNF-α mRNA level as well as

NLRP3 and NF-kb P65 protein expression. The similar changes were observed in Gr-1 staining assay, which was associated with functional neutrophils performance. There were many Gr-1 + neutrophils with brown-nuclear staining recruited into the infected mice heart in group (2). The fluorescence intensity of Gr-1$^+$ neutrophils was also decreased near 60% and 80% in group (5) and group (6). Apparently, group (3) and group (4) did not significantly changed from group (2), meaning that the PCM-MSN@LA + LIFU remarkably inhibit the functional neutrophil accumulation (Fig. 10g).

ROS generation was assessed using MDA and DHE immunofluorescence analyses. PCM-MSN@LA was delivered with LPS injection, could evidently decreased the cardiac content of MDA induced by LPS. The same decreases were observed in group (6) with the treatment of PCM-MSN@LA that contained LIFU irradiation (Fig. 11a). DHE assays showed the concomitant increases in oxidative stress in the myocardium of LPS treated mice, and PCM-MSN@LA significantly suppressed the effects. Moreover, the fewest ROS fluorescent intensity was found in group (6) under the treatment of PCM-MSN@LA with LIFU targeting. Collectively, PCM-MSN@LA + LIFU exhibited excellent antioxidant activity against ROS burden after myocardial injury in LPS induced sepsis model (Fig. 11b & c).

Drp1 and mfn2, are two mitochondrial regulatory enzymes that control mitochondrial fission and fusion (26, 27). Mitochondrial fission and fusion are closely related to mitochondrial function and influenced by LPS, evidenced as upregulation of drp1 expression and downregulation of mfn2 level compared to those of controls. PCM-MSN@LA treatment, but not PCM-MSN or MSN@LA, inhibited these effects. The combination treatment with LIFU further reduced the level of drp1 and increased the level of mfn2 (Fig. 12a & b). Consistently, broken and swollen cardiac muscle fibers, damaged mitochondria with various sizes, vacuolar changes and partial cristae disruptions were further observed by TEM (Fig. 12c). These changes were evidently attenuated in groups (5) and (6), which were treated with PCM-MSN@LA, especially in group (6) in addition to the LIFU irradiation. But, PCM-MSN and MSN@LA injection changed the mitochondrial appearance less, suggesting that PCM-MSN@LA + LIFU which could efficiently release NO in cardiac effectively restored mitochondrial function.

Discussion

Cardiac dysfunction is an early and fatal complication of sepsis (12). Even, the prevalence interest of NO therapy in cardiovascular developed, therapeutic NO for modulation of myocardial function in sepsis is not yet practiced. Because the drawback of NO is rapid diffusion (28). We developed the nontoxic and efficient NO donor delivery system (PCM-MSN@LA + LIFU) to control NO release during sepsis and promoted cardiac function injured by LPS. This is the first time to report the effect of targeted NO donor delivery system in septic cardiac.

The targeted delivery system is based on an MSN-conjugated 20-mer peptide, named PCM, with excellent binding capacity to the heart. It was demonstrated by apparently more FITC-stained PCM-MSN affinity to cardiomyocytes in vitro compared to scramble peptide MSNs. Similar results were obtained in vivo, a 7-fold increase in the intensity of red regions of Cy5.5-stained PCM-MSN nanoparticles located in cardiac

tissue compared to scramble peptide MSNs. Besides, in vitro, the PCM-MSN nanoparticles preferentially bound to cardiomyocytes but not HepG2 cells. Similarly, in vivo, 3 times stronger fluorescent PCM-MSN signals were distributed in the heart compared to other important organs, which suggesting that PCM efficiently guides nanoparticles to the heart, and thus enhances tissue-specific uptake in consistent with previously research (15, 16, 29, 30). Analog to our results, Michael J et al. developed a quantitative real-time PCR assay to show that PCM had a nearly 50-fold increase in selectivity for the heart over control 20-mer peptides (15). Other advantages of peptide include lower molecular weight, easier synthesis, lower cytotoxicity and better conjugation to nanocarriers than any other antibody (14). A LIFU-triggered drug delivery system could be an alternative method for liberating drug on focused site. Ultrasound with high US energy, called high-intensity focused US (HIFU), only induces restricted delivery to the heart. Conversely, noninvasive LIFU, with low energy, exhibits considerable tissue-penetrating ability. Thus, it has been intensively studied for therapy and imaging diagnosis (16–18, 31). Consistent with the optimum frequency, we set 1.0 W/cm^2-20% power as our LIFU parameter (19). Irradiated by LIFU upon the heart, PCM-MSN@LA successfully penetrated into the cardiac tissue and released more NO without inducing prominent side effects on the circulation.

Another issue of concern was the level of NO production. NO is produced in various cells by the NOS isoforms, which generates NO through the oxidation of LA. NO deficiency is critically associated with the onset and development of cardiovascular disease (10, 32). In our results, NO generation in situ was demonstrated as following: different doses of PCM-MSN@LA, even under the LIFU irradiation, induced few changes on NO levels in cardiomyocytes without any treatment. Because, in normal cases, the expressions of eNOS are few, so NO generation does not show significant changes. However, in the sepsis environment, with the increase of iNOS and eNOS, NO generation is closely related to PCM-MSN@LA, which indicates that our materials generate NO in specific environments and act on the body. Secondly, data from the UV–vis assay showed that exposure to LIFU irradiation, 25.6% of LA leaked from PCM-MSN@LA nanoparticles in pH 7.35–7.45 solutions. Even in pH 7.00-7.30 solution, the leakage was only 35.3%, confirming the high stability of PCM-MSN@LA. We deduced this result was primarily due to the strong electrostatic affinity between PCM-MSNs and LA molecules. On the basis of LA release, NO generation from PCM-MSN@LA + LIFU treatment in the acidic septic microenvironment was similarly low. The biological effects of NO highly rely on the concentration of NO (33). The considerably low level of NO is associated with some of the most important immunopathologies in the cardiovascular disease and exert effectiveness to cardiovascular dysfunction. (10, 25, 34). Thus, the infective microenvironment responsive sequential generation of NO system accomplished in our research paves the way for cardiac therapy.

Finally, our data clearly showed a central role of NO in inhibiting cardiomyocyte apoptosis and ameliorating cardiac function in severe sepsis. The therapeutic effects of myocardium-targeted NO-releasing nanoparticles in sepsis models relied on immune regulation, ROS reduction and mitochondrial modulation. Our data showed that PCM-MSN@LA + LIFU treatment remarkably decreased excessive cytokines secretion. In consistent with previous research (35, 36), both NLRP3 and NF-κB p65, high expressed in septic mice, were also reduced after PCM-MSN@LA + LIFU treatment. NLRP3 and NF-κB P65

were two important components of the inflammasome after LPS injection. Stimulation of NF-κB P65 together with activation of NLRP3, cardiac dysfunction ensue (37). Thus, downregulation of NLRP3 and NF-κB expression accompanied with inhibition of proinflammatory cytokines could efficiently improve the heart function. Furthermore, there were significantly fewer Gr-1-positive neutrophils in the PCM-MSN@LA + LIFU group than the other groups, meaning that NO played a central role in neutrophil migration.

LPS leads to the elevation of oxidative stress, which promotes the proinflammatory immune reaction and causes severe damage to mitochondrial metabolism (7, 38). Indeed, the reduction of NO bioavailability are also associated with excessive ROS generation. Therefore, we assume that NO production was enough to tip the balance, NO bioactivity was retained. Bioactive NO, in turn, modulate NADPH oxidase, regulate cardiac mitochondrial respiration and keep the heart away from neutrophil infiltration, further mitigating the ROS burden (25, 39–42). As it were predicted, the application of PCM-MSN@LA + LIFU simultaneously with LPS, liberating bioactive NO on myocardium, exhibited a robust inhibitory effect on LPS-induced oxidative stress. The MDA contents were carried out with DHE assays to confirm the antioxidant effect. PCM-MSN@LA + LIFU treatment reduced the MDAs levels compared with LPS group. The same results were observed in photographs of DHE staining of heart sections. PCM-MSN@LA + LIFU treatment significantly decreased the number of DHE-positive cells compared with LPS group.

The mitochondrial density in cardiomyocytes is high, which allows them to produce energy quickly (4). Mitochondrial dysfunction in sepsis were demonstrated as elevated Mfn2 expression and diminished Drp1 expression. PCM-MSN@LA + LIFU exert mitochondrial protection by diminishing the Mfn2 as well as elevating the Drp1 expression. We also noted that the morphology and density were improved after PCM-MSN@LA + LIFU injection by TEM images.

Despite several decades of research regarding the effect of NO donor in sepsis, the clinical use of NO to treat septic hearts is limited. The point is that vasodilatory action induced by NO further accelerate hemodynamic collapse (20). Notably, unlike MSN@LA treatment lowered blood pressure, PCM-MSN@LA, in response to LIFU irradiation, quickly accumulated in the septic heart and avoid the blood pressure collapses. Thus, precise myocardium-targeted NO-producing nanoparticles successfully avoided the side effects of NO diffusion and resulted in myocardial protection.

Unfortunately, the imaging-guided monitoring delivery system of gas in vivo is still a challenge, we could not observe the whole process of NO liberation to the heart. we are going to address it next.

Conclusion

Overall, the myocardial delivery of NO donor was accomplished by PCM and LIFU guide. Responsive of infective microenvironment, the PCM-MSN@LA successfully generate NO. This precise gas therapy exerts excellent benefits for myocardial function improvement, providing a new treatment to modulate the microenvironment in sepsis-induced myocardial injury.

Declarations

Authors'contributions:

MO and ZZ conceived and designed the experiments. MO wrote the manuscript. XO and ZP executed the experiments, analyzed the data.   GX, QS, and MZ edited the manuscript. HL and ZZ supervised the project and made the final approval of the manuscript.

All authors read and approved the final manuscript.

Availability of data and materials:

All data generated or analyzed during this study are included in this published article.

Ethics approval and consent to participate:

All institutional and national guidelines for the care and use of laboratory animals were followed. All the animal care and experimental protocols were carried out with review and approval from the Laboratory Animal Welfare and Ethics Committee of Central South University

Consent for publication:

All authors agree to be published.

Competing interests

The authors declare no conflict of interest.

References

1. Adhikari NK, Fowler RA, Bhagwanjee S, Rubenfeld GD. Critical care and the global burden of critical illness in adults. *Lancet* 2010; 376 9749 : 1339-1346.

2. Rudd KE, Johnson SC, Agesa KM, Shackelford KA, Tsoi D, Kievlan DR, Colombara DV, Ikuta KS, Kissoon N, Finfer S, Fleischmann-Struzek C, Machado FR, Reinhart KK, Rowan K, Seymour CW,

Watson RS, West TE, Marinho F, Hay SI, Lozano R, Lopez AD, Angus DC, Murray CJL, Naghavi M. Global, regional, and national sepsis incidence and mortality, 1990-2017: analysis for the Global Burden of Disease Study. *Lancet* 2020; 395 10219 : 200-211.

3. Gupta RK, Harrison EM, Ho A, Docherty AB, Knight SR, van Smeden M, Abubakar I, Lipman M, Quartagno M, Pius R, Buchan I, Carson G, Drake TM, Dunning J, Fairfield CJ, Gamble C, Green CA, Halpin S, Hardwick HE, Holden KA, Horby PW, Jackson C, McLean KA, Merson L, Nguyen-Van-Tam JS, Norman L, Olliaro PL, Pritchard MG, Russell CD, Scott-Brown J, Shaw CA, Sheikh A, Solomon T, Sudlow C, Swann OV, Turtle L, Openshaw PJM, Baillie JK, Semple MG, Noursadeghi M, Investigators IC. Development and validation of the ISARIC 4C Deterioration model for adults hospitalised with COVID-19: a prospective cohort study. *The Lancet Respiratory medicine* 2021; 9 4 : 349-359.

4. Lin H, Wang W, Lee M, Meng Q, Ren H. Current Status of Septic Cardiomyopathy: Basic Science and Clinical Progress. *Frontiers in pharmacology* 2020; 11 : 210.

5. Ehrman RR, Moore SC, Favot MJ, Akers KG, Gallien JZ, Welch RD, Abidov A, Sherwin RL, Levy PD. Scientific Letter to the Editor: Need for a Definitive Study of Global Longitudinal Strain for Prognostication in Septic Cardiomyopathy. *Journal of the American Society of Echocardiography : official publication of the American Society of Echocardiography* 2019; 32 4 : 549-552 e543.

6. Ehrman RR, Sullivan AN, Favot MJ, Sherwin RL, Reynolds CA, Abidov A, Levy PD. Pathophysiology, echocardiographic evaluation, biomarker findings, and prognostic implications of septic cardiomyopathy: a review of the literature. *Critical care* 2018; 22 1 : 112.

7. Martin L, Derwall M, Al Zoubi S, Zechendorf E, Reuter DA, Thiemermann C, Schuerholz T. The Septic Heart: Current Understanding of Molecular Mechanisms and Clinical Implications. *Chest* 2019; 155 2 : 427-437.

8. Khambata RS, Ghosh SM, Rathod KS, Thevathasan T, Filomena F, Xiao Q, Ahluwalia A. Antiinflammatory actions of inorganic nitrate stabilize the atherosclerotic plaque. *Proceedings of the National Academy of Sciences of the United States of America* 2017; 114 4 : E550-E559.

9. Kim YM, Talanian RV, Li J, Billiar TR. Nitric oxide prevents IL-1beta and IFN-gamma-inducing factor (IL-18) release from macrophages by inhibiting caspase-1 (IL-1beta-converting enzyme). *Journal of immunology* 1998; 161 8 : 4122-4128.

10. Carlstrom M, Montenegro MF. Therapeutic value of stimulating the nitrate-nitrite-nitric oxide pathway to attenuate oxidative stress and restore nitric oxide bioavailability in cardiorenal disease. *Journal of internal medicine* 2019; 285 1 : 2-18.

11. Angus DC, van der Poll T. Severe sepsis and septic shock. *The New England journal of medicine* 2013; 369 9 : 840-851.

12. Beesley SJ, Weber G, Sarge T, Nikravan S, Grissom CK, Lanspa MJ, Shahul S, Brown SM. Septic Cardiomyopathy. *Critical care medicine* 2018; 46 4 : 625-634.

13. Huang Z, Fu J, Zhang Y. Nitric Oxide Donor-Based Cancer Therapy: Advances and Prospects. *Journal of medicinal chemistry* 2017; 60 18 : 7617-7635.

14. Mousavizadeh A, Jabbari A, Akrami M, Bardania H. Cell targeting peptides as smart ligands for targeting of therapeutic or diagnostic agents: a systematic review. *Colloids and surfaces B, Biointerfaces* 2017; 158 : 507-517.

15. McGuire MJ, Samli KN, Johnston SA, Brown KC. In vitro selection of a peptide with high selectivity for cardiomyocytes in vivo. *Journal of molecular biology* 2004; 342 1 : 171-182.

16. Zhao X, Luo W, Hu J, Zuo L, Wang J, Hu R, Wang B, Xu L, Li J, Wu M, Li P, Liu L. Cardiomyocyte-targeted and 17beta-estradiol-loaded acoustic nanoprobes as a theranostic platform for cardiac hypertrophy. *Journal of nanobiotechnology* 2018; 16 1 : 36.

17. Sun Z, Xie Y, Lee RJ, Chen Y, Jin Q, Lv Q, Wang J, Yang Y, Li Y, Cai Y, Wang R, Han Z, Zhang L, Xie M. Myocardium-targeted transplantation of PHD2 shRNA-modified bone mesenchymal stem cells through ultrasound-targeted microbubble destruction protects the heart from acute myocardial infarction. *Theranostics* 2020; 10 11 : 4967-4982.

18. Liu J, Shang T, Wang F, Cao Y, Hao L, Ren J, Ran H, Wang Z, Li P, Du Z. Low-intensity focused ultrasound (LIFU)-induced acoustic droplet vaporization in phase-transition perfluoropentane nanodroplets modified by folate for ultrasound molecular imaging. *International journal of nanomedicine* 2017; 12 : 911-923.

19. Wang Y, Sui G, Teng D, Wang Q, Qu J, Zhu L, Ran H, Wang Z, Jin C, Wang H. Low intensity focused ultrasound (LIFU) triggered drug release from cetuximab-conjugated phase-changeable nanoparticles for precision theranostics against anaplastic thyroid carcinoma. *Biomaterials science* 2018; 7 1 : 196-210.

20. Li M, Li J, Chen J, Liu Y, Cheng X, Yang F, Gu N. Platelet Membrane Biomimetic Magnetic Nanocarriers for Targeted Delivery and in Situ Generation of Nitric Oxide in Early Ischemic Stroke. *ACS nano* 2020; 14 2 : 2024-2035.

21. Yang F, Li M, Liu Y, Wang T, Feng Z, Cui H, Gu N. Glucose and magnetic-responsive approach toward in situ nitric oxide bubbles controlled generation for hyperglycemia theranostics. *Journal of controlled release : official journal of the Controlled Release Society* 2016; 228 : 87-95.

22. Zhang K, Xu H, Jia X, Chen Y, Ma M, Sun L, Chen H. Ultrasound-Triggered Nitric Oxide Release Platform Based on Energy Transformation for Targeted Inhibition of Pancreatic Tumor. *ACS nano* 2016; 10 12 : 10816-10828.

23. Fan W, Lu N, Huang P, Liu Y, Yang Z, Wang S, Yu G, Liu Y, Hu J, He Q, Qu J, Wang T, Chen X. Glucose-Responsive Sequential Generation of Hydrogen Peroxide and Nitric Oxide for Synergistic Cancer Starving-Like/Gas Therapy. *Angewandte Chemie* 2017; 56 5 : 1229-1233.

24. Farah C, Michel LYM, Balligand JL. Nitric oxide signalling in cardiovascular health and disease. *Nature reviews Cardiology* 2018; 15 5 : 292-316.

25. Jackson J, Patterson AJ, MacDonald-Wicks L, McEvoy M. The role of inorganic nitrate and nitrite in CVD. *Nutrition research reviews* 2017; 30 2 : 247-264.

26. van der Bliek AM, Shen Q, Kawajiri S. Mechanisms of mitochondrial fission and fusion. *Cold Spring Harbor perspectives in biology* 2013; 5 6 .

27. Sakaguchi A, Kimura W. Metabolic regulation of cardiac regeneration: roles of hypoxia, energy homeostasis, and mitochondrial dynamics. *Current opinion in genetics & development* 2021; 70：54-60.

28. Lundberg JO, Gladwin MT, Weitzberg E. Strategies to increase nitric oxide signalling in cardiovascular disease. *Nature reviews Drug discovery* 2015; 14 9：623-641.

29. Rana S, Datta K, Reddy TL, Chatterjee E, Sen P, Pal-Bhadra M, Bhadra U, Pramanik A, Pramanik P, Chawla-Sarkar M, Sarkar S. A spatio-temporal cardiomyocyte targeted vector system for efficient delivery of therapeutic payloads to regress cardiac hypertrophy abating bystander effect. *Journal of controlled release : official journal of the Controlled Release Society* 2015; 200：167-178.

30. Kanki S, Jaalouk DE, Lee S, Yu AY, Gannon J, Lee RT. Identification of targeting peptides for ischemic myocardium by in vivo phage display. *Journal of molecular and cellular cardiology* 2011; 50 5：841-848.

31. Zhao YZ, Zhang M, Wong HL, Tian XQ, Zheng L, Yu XC, Tian FR, Mao KL, Fan ZL, Chen PP, Li XK, Lu CT. Prevent diabetic cardiomyopathy in diabetic rats by combined therapy of aFGF-loaded nanoparticles and ultrasound-targeted microbubble destruction technique. *Journal of controlled release : official journal of the Controlled Release Society* 2016; 223：11-21.

32. Dezfulian C, Shiva S, Alekseyenko A, Pendyal A, Beiser DG, Munasinghe JP, Anderson SA, Chesley CF, Vanden Hoek TL, Gladwin MT. Nitrite therapy after cardiac arrest reduces reactive oxygen species generation, improves cardiac and neurological function, and enhances survival via reversible inhibition of mitochondrial complex I. *Circulation* 2009; 120 10：897-905.

33. Thomas DD, Ridnour LA, Isenberg JS, Flores-Santana W, Switzer CH, Donzelli S, Hussain P, Vecoli C, Paolocci N, Ambs S, Colton CA, Harris CC, Roberts DD, Wink DA. The chemical biology of nitric oxide: implications in cellular signaling. *Free radical biology & medicine* 2008; 45 1：18-31.

34. Cauwels A, Buys ES, Thoonen R, Geary L, Delanghe J, Shiva S, Brouckaert P. Nitrite protects against morbidity and mortality associated with TNF- or LPS-induced shock in a soluble guanylate cyclase-dependent manner. *The Journal of experimental medicine* 2009; 206 13：2915-2924.

35. Mao K, Chen S, Chen M, Ma Y, Wang Y, Huang B, He Z, Zeng Y, Hu Y, Sun S, Li J, Wu X, Wang X, Strober W, Chen C, Meng G, Sun B. Nitric oxide suppresses NLRP3 inflammasome activation and protects against LPS-induced septic shock. *Cell research* 2013; 23 2：201-212.

36. Connelly L, Palacios-Callender M, Ameixa C, Moncada S, Hobbs AJ. Biphasic regulation of NF-kappa B activity underlies the pro- and anti-inflammatory actions of nitric oxide. *Journal of immunology* 2001; 166 6：3873-3881.

37. Toldo S, Mezzaroma E, McGeough MD, Pena CA, Marchetti C, Sonnino C, Van Tassell BW, Salloum FN, Voelkel NF, Hoffman HM, Abbate A. Independent roles of the priming and the triggering of the NLRP3 inflammasome in the heart. *Cardiovascular research* 2015; 105 2：203-212.

38. Tsolaki V, Makris D, Mantzarlis K, Zakynthinos E. Sepsis-Induced Cardiomyopathy: Oxidative Implications in the Initiation and Resolution of the Damage. *Oxidative medicine and cellular longevity* 2017; 2017：7393525.

39. Sui Y, Tian R, Lu N. NADPH oxidase is a primary target for antioxidant effects by inorganic nitrite in lipopolysaccharide-induced oxidative stress in mice and in macrophage cells. *Nitric oxide : biology and chemistry* 2019; 89：46-53.

40. Qian J, Chen F, Kovalenkov Y, Pandey D, Moseley MA, Foster MW, Black SM, Venema RC, Stepp DW, Fulton DJ. Nitric oxide reduces NADPH oxidase 5 (Nox5) activity by reversible S-nitrosylation. *Free radical biology & medicine* 2012; 52 9：1806-1819.

41. Bryan NS, Calvert JW, Gundewar S, Lefer DJ. Dietary nitrite restores NO homeostasis and is cardioprotective in endothelial nitric oxide synthase-deficient mice. *Free radical biology & medicine* 2008; 45 4：468-474.

42. Graham DB, Jasso GJ, Mok A, Goel G, Ng ACY, Kolde R, Varma M, Doench JG, Root DE, Clish CB, Carr SA, Xavier RJ. Nitric Oxide Engages an Anti-inflammatory Feedback Loop Mediated by Peroxiredoxin 5 in Phagocytes. *Cell reports* 2018; 24 4：838-850.

Figures
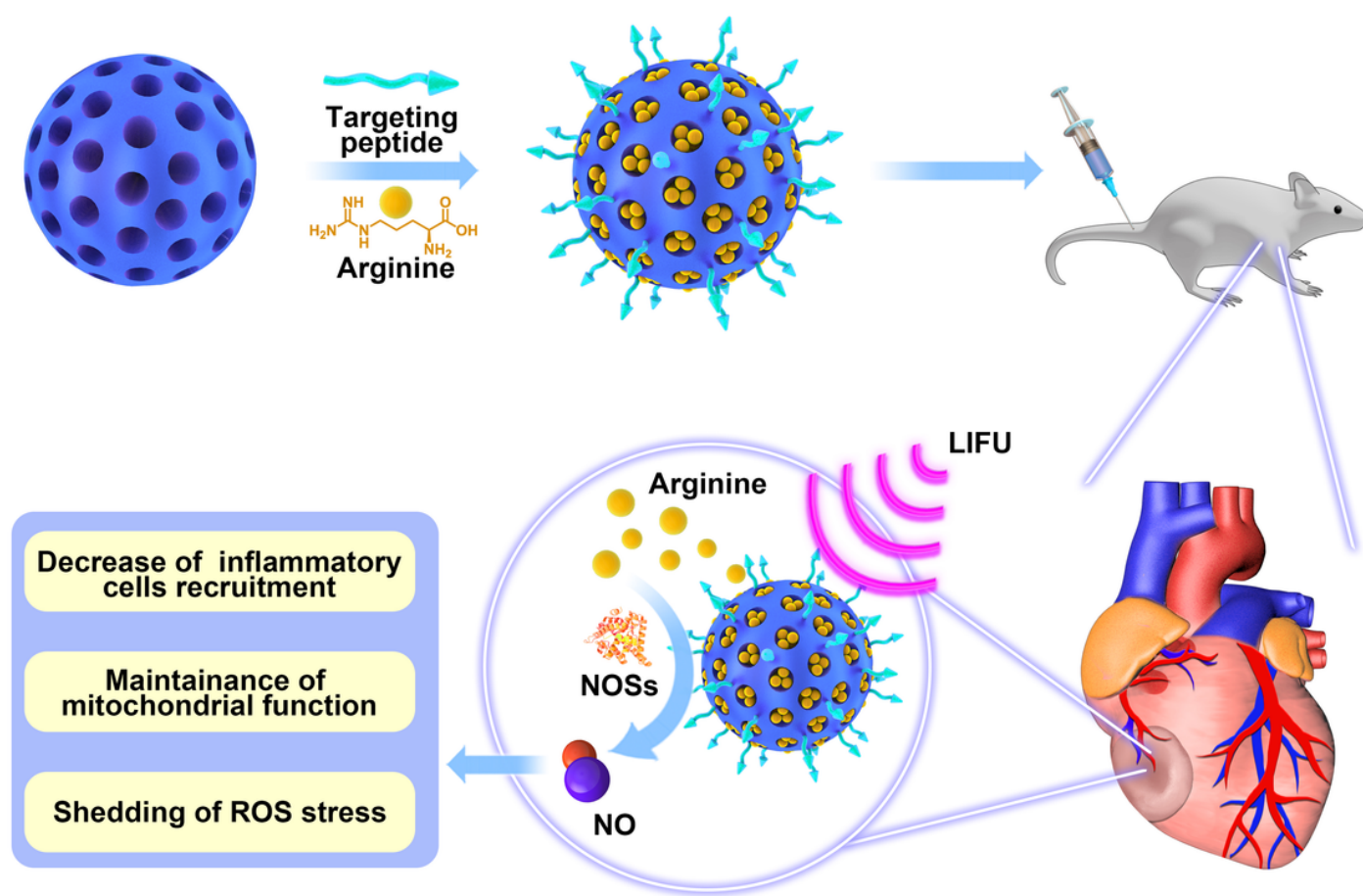
Figure 1

NO liberation in septic heart from PCM-carried and L-arginine loaded porous MSN, named PCM-MSN@LA ,combined with the LIFU, preventing the myocardial dysfunction.
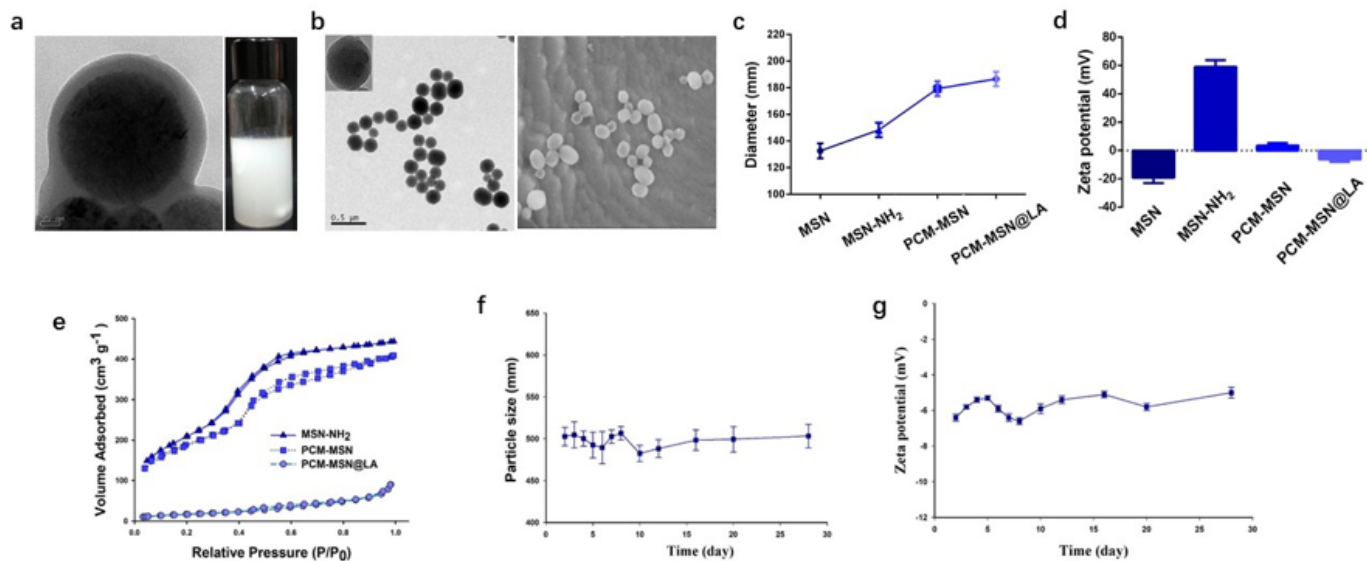
Figure 2

Physicochemical characterization of PCM-MSN@LA. a TEM images of PCM-MSN@LA particles and the appearance of PCM-MSN@LA particles (scale bar=20nm). b TEM and SEM images of PCM-MSN@LA particles (scale bar=0.5μm). Variation of MSNs after each modification in c size and d zeta. e Specific surface area of different samples analyzed by N2 adsorption-desorption method. f, g The variation of particle in size and zeta of PCM-MSN@LA in deionized water from 0 days to 28 days measured using DLS.
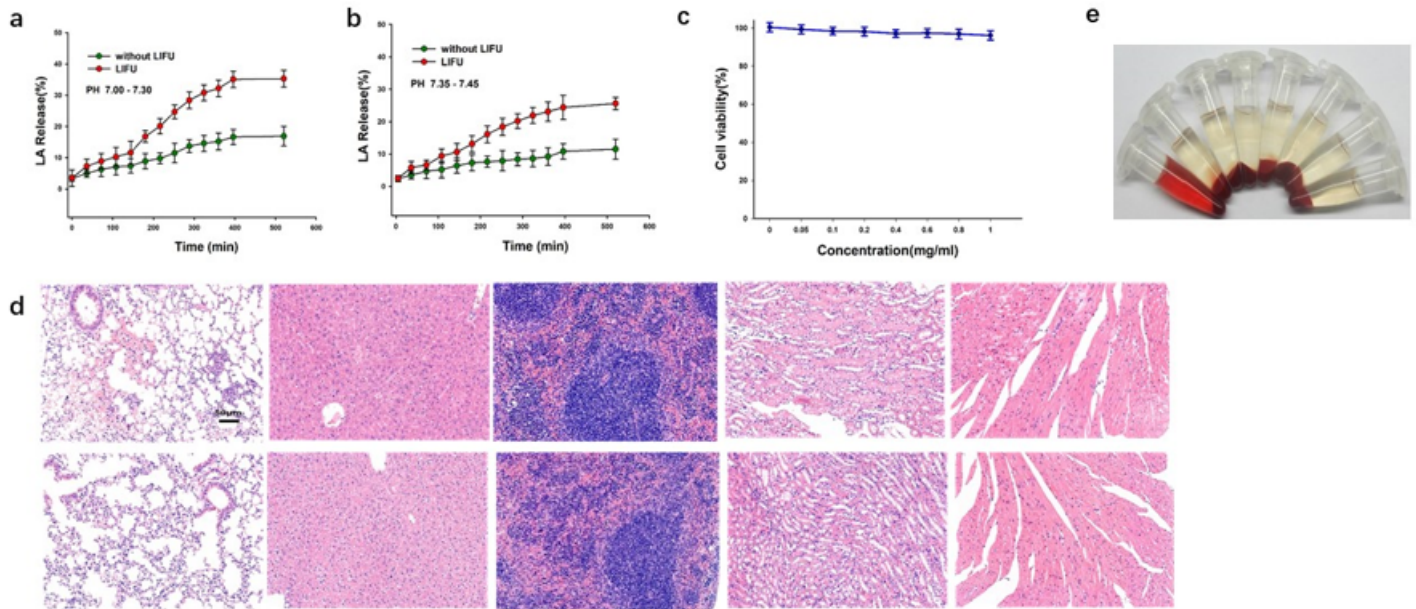
Figure 3

The L-arginine releasing efficiency and the safety of PCM-MSN@LA. L-arginine released from PCM-MSN@LA with or without LIFU irradiation (1.0W/cm2) in deionized water with a PH 7.00-7.30 and b PH 7.35-7.45. c Relative viability of cardiomyocytes 24h after incubated with different concentrations of PCM-MSN@LA. d The HE stained images of the lung, liver, spleen, kidney, and heart before and 24h after administration of 50mg/kg PCM-MSN@LA (scale bar=50μm). e Photographs of RBCs incubated with PCM-MSN@LA particles at different concentrations ranging from 25 to 3200 mg ml-1 for 3h.
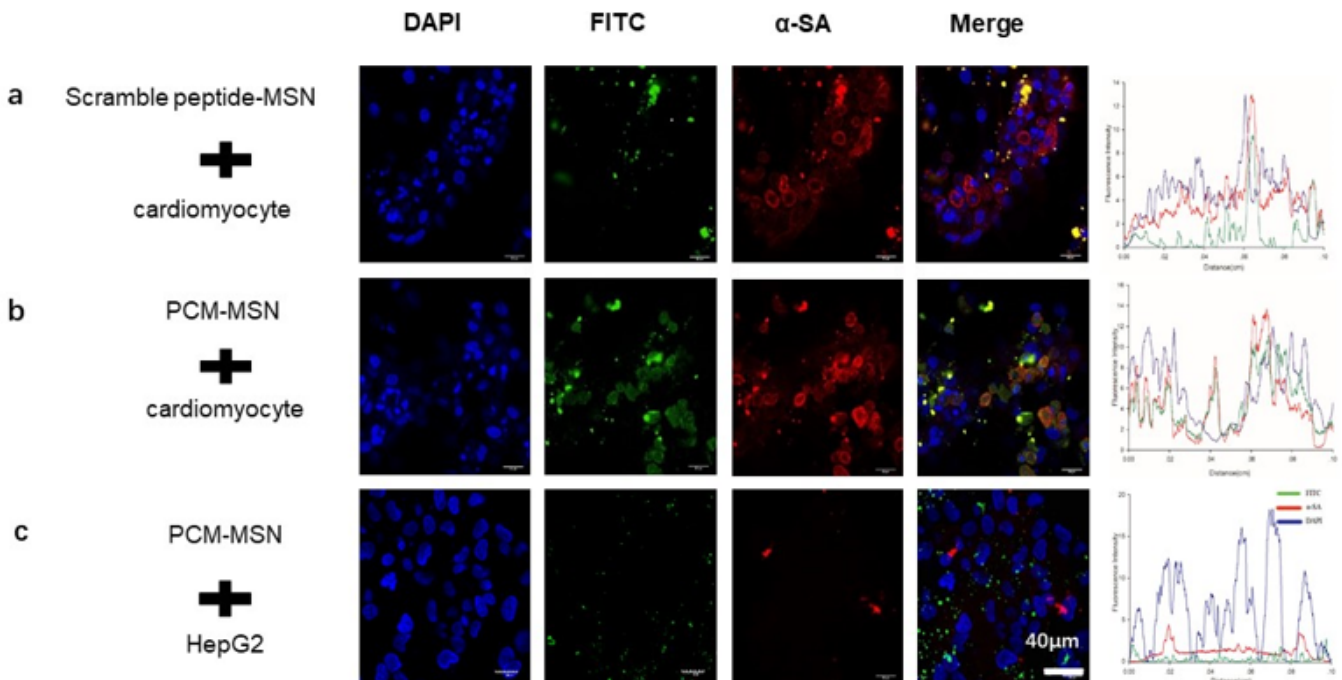
Figure 4

Specificity of PCM in Cardiomyocytes in vitro. a, b Immunofluorescence staining and fluorescence intensity of cardiomyocytes after incubated with a scramble peptide-MSN and b PCM-MSN for 1h. c Immunofluorescence staining and fluorescence intensity of HepG2 after incubated with PCM-MSN for 1h. DAPI (blue; nuclei), FITC (green; PCM or scramble peptide), α-SA (red; cardiomyocyte) (scale Bar = 40μm; n = 6 per group).
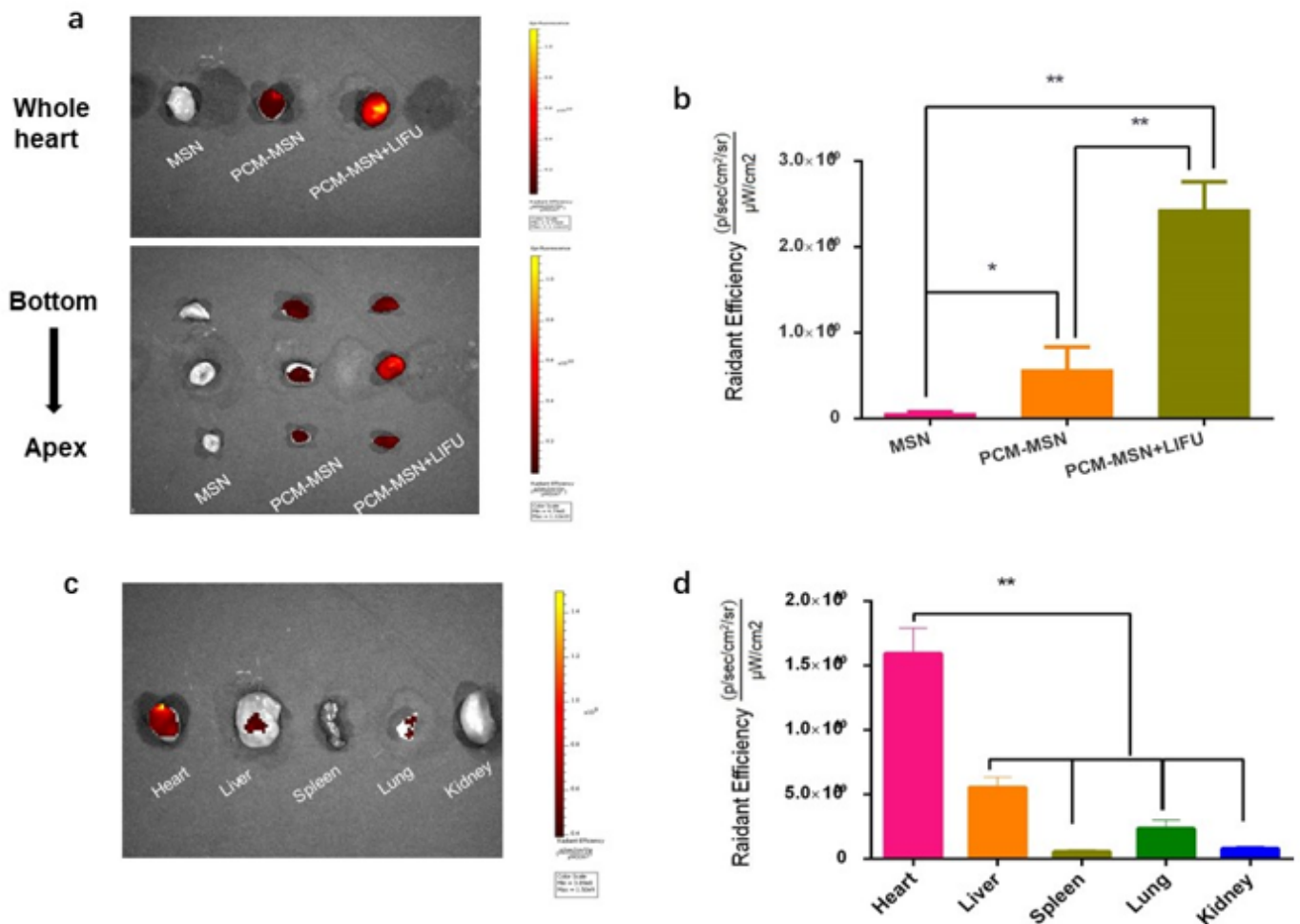
Figure 5

Cardiac specificity of PCM-MSN+LIFU in vivo. a Immunofluorescence study showing delivery efficiency of Cy5.5-stained MSN, Cy5.5-stained PCM-MSN with or without LIFU to the heart 6h after individualized treatments (n = 4 per group). b Fluorescence intensity analysis after individualized treatments (*p 0.05, **p 0.01). c Accumulation of Cy5.5-stained PCM-MSN observed in the heart and other organs after LIFU irradiation (n = 4 per group). d Quantitative distributions of merged florescence intensity in different organs (**p 0.01)
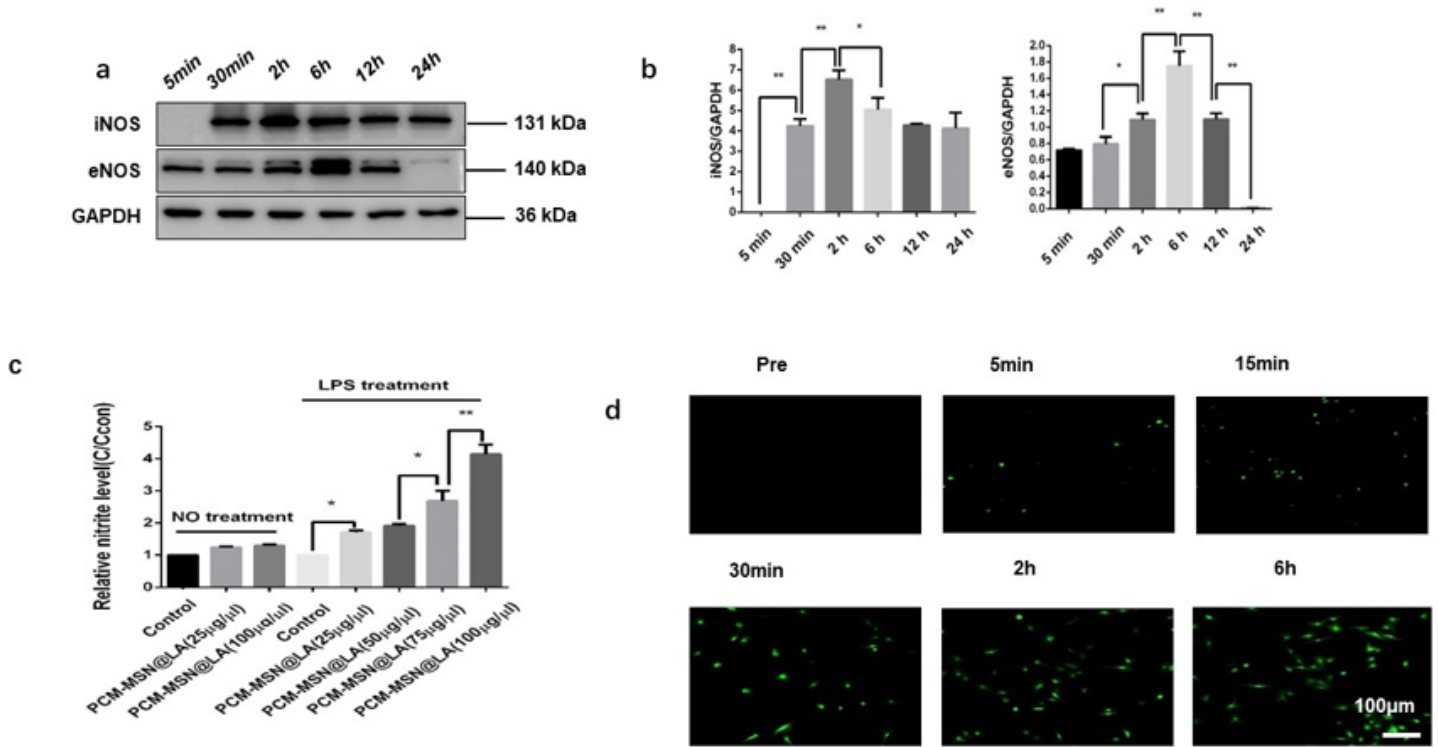
Figure 6

Assessment of NO generation from PCM-MSN@LA with or without LIFU in vitro. a The expression of iNOS and eNOS in LPS incubated cardiomyocytes from 5min to 24h. b The quantitative analyses of iNOS and eNOS expression (n=6, per group, *p 0.05; **p 0.01). c Relative nitrite concentration from different doses of PCM-MSN@LA in cardiomyocytes with or without LPS (n = 6 per group, *p 0.05; **p 0.01). d Confocal images of cardiomyocytes stained by DAF-FM DA following 75µg/ml PCM-MSN@LA irradiated with LIFU over time (scale bar=100 µm)
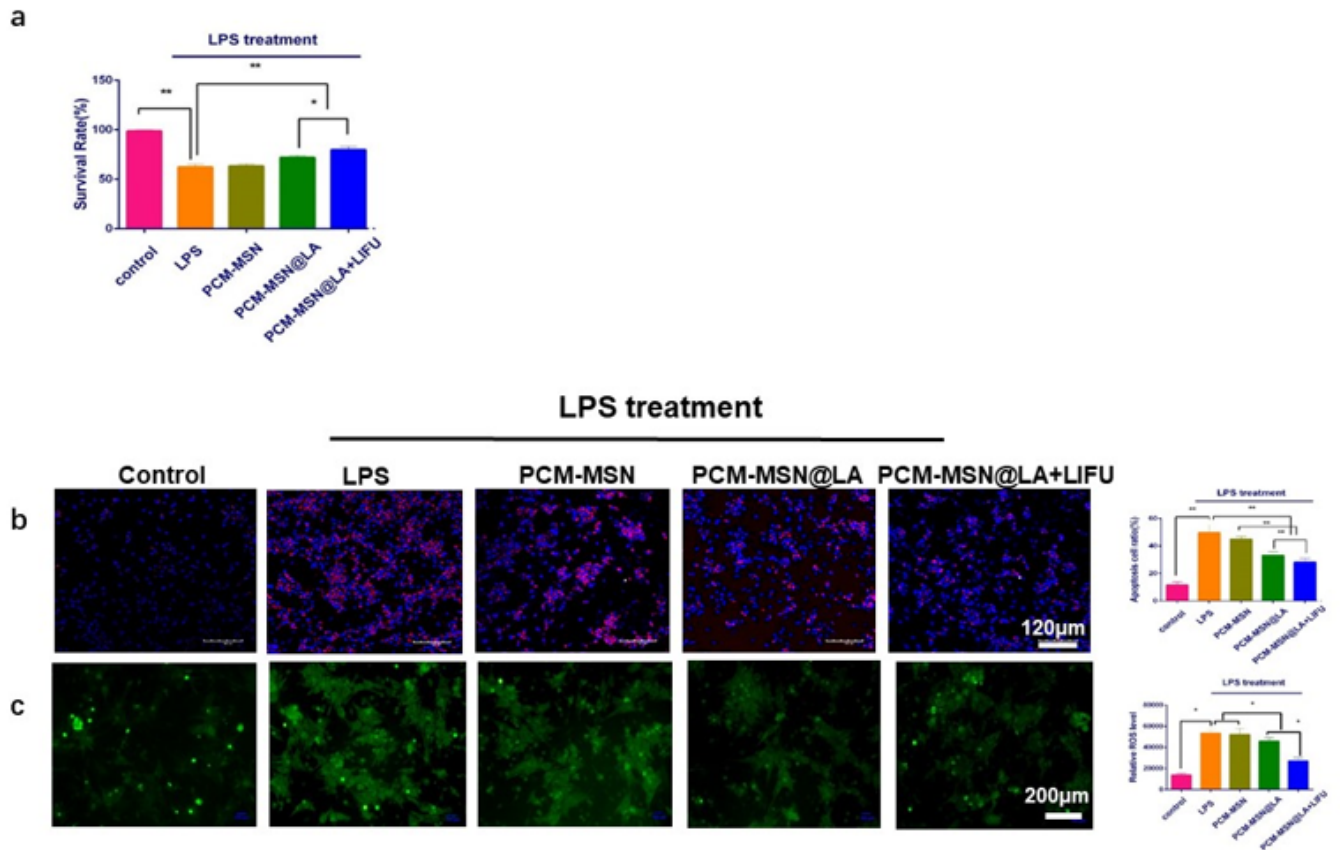
Figure 7

NO reduced cardiomyocyte apoptosis. a Cell viability of each modality of treatments (n=6, per group, *p 0.05; **p 0.01). b Photomicrographs of cardiomyocyte apoptosis after TUNEL staining and quantitative analysis of cell apoptosis rate (scale bar=120 μm; n=6 per group, *p 0.05; **p 0.01). c. Confocal images of cardiomyocyte stained by DCFH-DA after individualized treatments and the quantitative analysis of the ratio of ROS fluorescence intensity (scale bar=200 μm; n=6 per group, *p 0.05; **p 0.01).
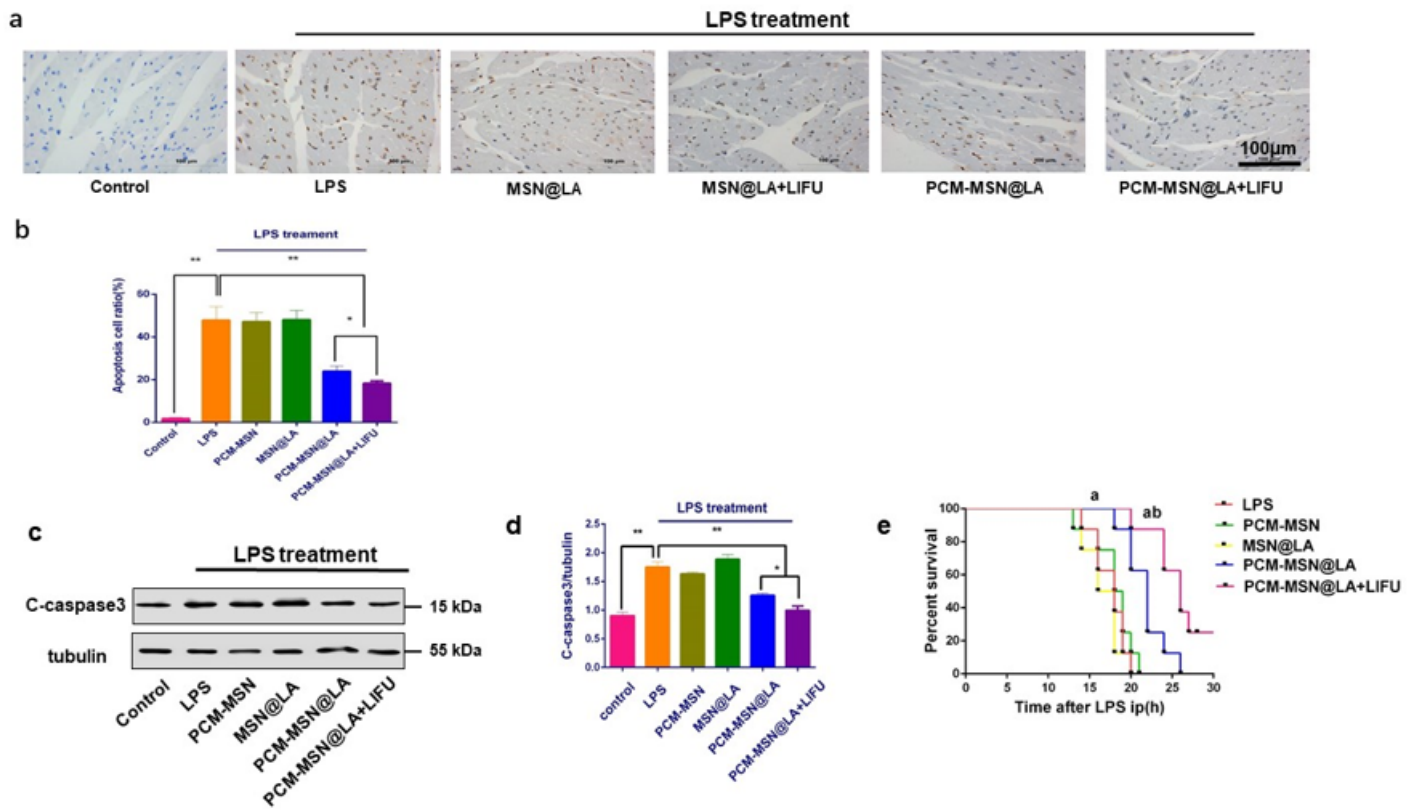
Figure 8

Myocardium-targeted NO release significantly attenuated LPS-induced cardiomyocyte apoptosis and decreased the expression of caspase 3 in cardiac tissues. a TUNEL assay of cardiomyocytes from different modalities (scale bar=100 μm) . b Quantitative analysis of apoptotic cells ratio by counting the TUNEL-positive cells (n=8 per group). Data were presented as Mean±SD. *p 0.05; **p 0.01. c, d The expression and quantitative analysis of caspase 3 (n=8 per group). Data were presented as Mean±SD. *p 0.05; **p 0.01. e Survival rate during severe sepsis. aP<0.05 vs. CLP; bP<0.05 vs. PCM-MSN@LA.
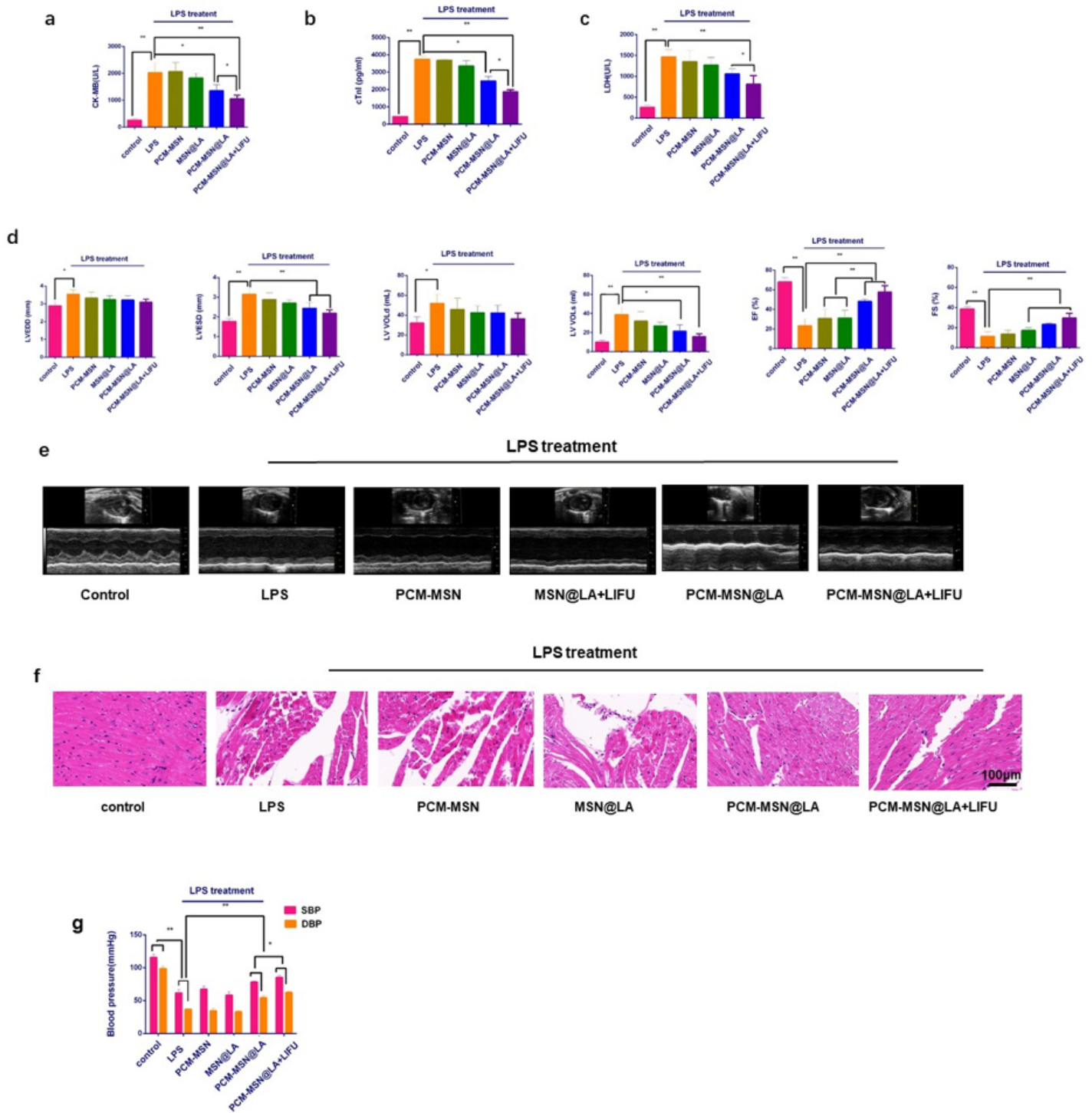
Figure 9

Myocardium-targeted NO release prevented heart dysfunction. a-c The clinical markers in serum of mice in different groups (n=8 per group). d Serials of echocardiographic assessments of LV function in murine models of different experimental groups (n=8 per group). LVIDd, left ventricular internal diameter at the end of diastole; LVIDs, left ventricular internal diameter at the end of systole; LV VOL d, Left volumes at the end diastole; LV VOL s, Left volumes at the end systole; EF, ejection fraction; FS, fraction shorting.

*P<0.05; **P<0.01. e Representative M-mode echocardiograms were presented in parasternal short-axis view (at the level of papillary muscle) for FS and EF measurement following different treatments. f The representation of morphological changes shown by HE staining before and after different treatments (n=8 per group; scale bar=100μm). g The change of blood pressure induced by different treatments (n=8 per group). SBP, systolic blood pressure; DBP, diastolic blood pressure.
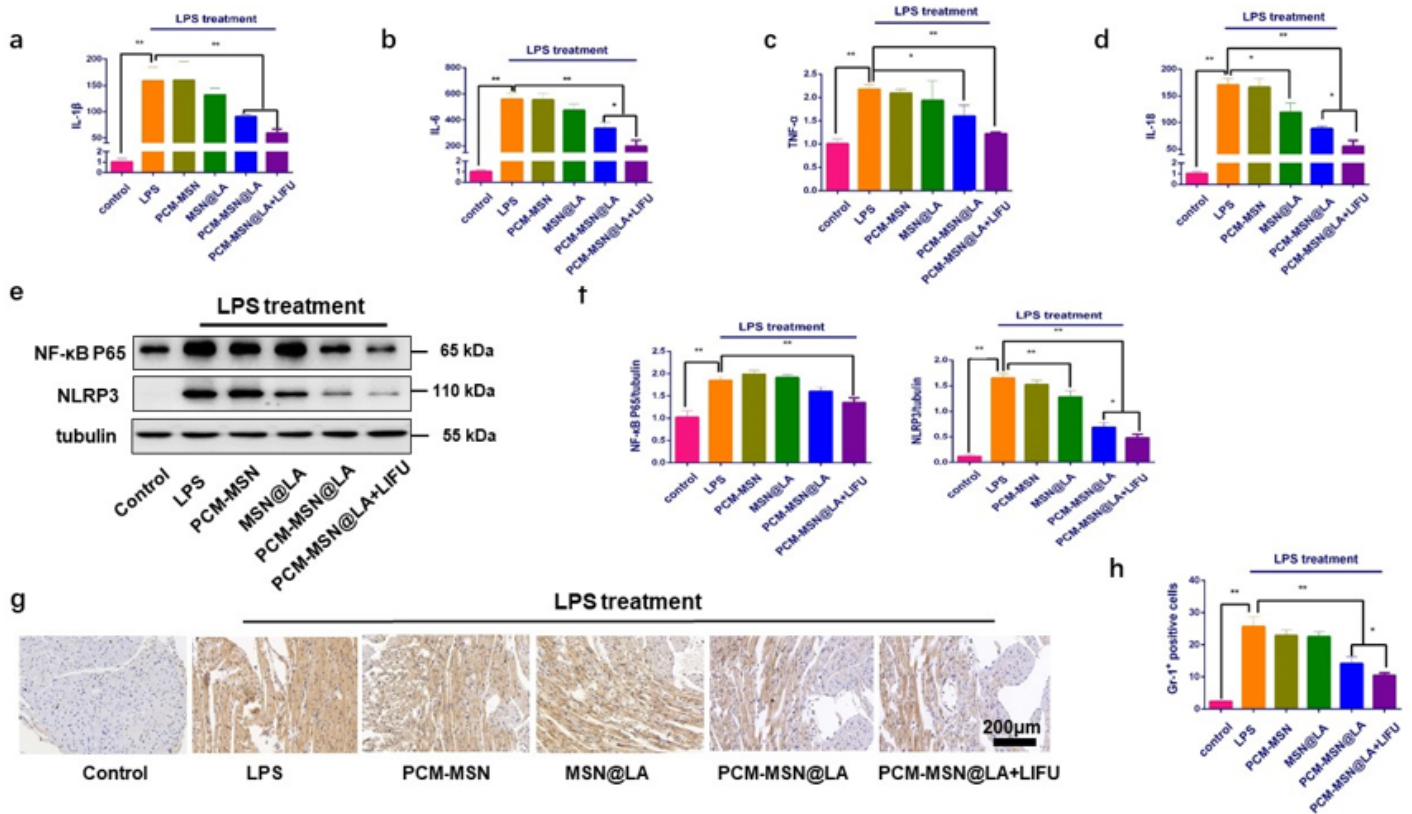

Figure 10

Myocardium-targeted NO release effectively regressed LPS-induced myocardial pro-inflammatory response. a-d Inflammatory cytokines including IL-1, IL-6, IL-18, and TNF-α in serums measured 6h after different treatments (n=8 per group; Data were presented as Mean±SD. *P<0.01; **P<0.05). e The expression of inflammatory mediator proteins NLRP3 and NF-κB P65. f The quantitative analysis of NLRP3 and NF-κB P65 proteins expression. g Optical microscopic images of cardiac tissue slices stained by Gr-1+ immunohistochemistry (n=8 per group; scale bar=200μm). h The percentage of Gr-1+ positive cells in heart tissues (n=8 per group; Data were presented as Mean±SD. *P<0.01; **P<0.05).
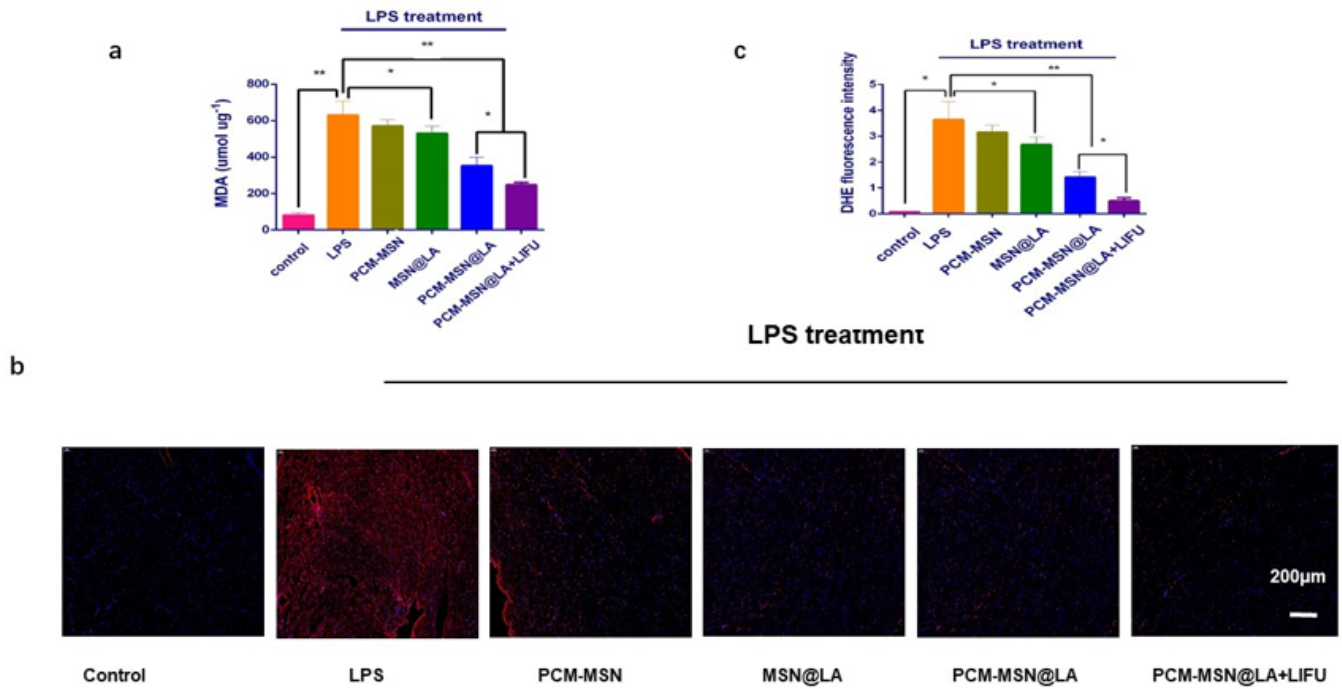
Figure 11

Myocardium-targeted NO release effectively relieved LPS-induced myocardial antioxidants stress. a MDA concentration produced in different groups. b Graphs showing the ROS fluorescent probe-DHE stained sections in the heart (n=8 per group; scale bar=200μm). c The quantitative analysis of ROS fluorescent intensity (n=8 per group; Data are presented as Mean±SD. *P<0.05; **P<0.01).
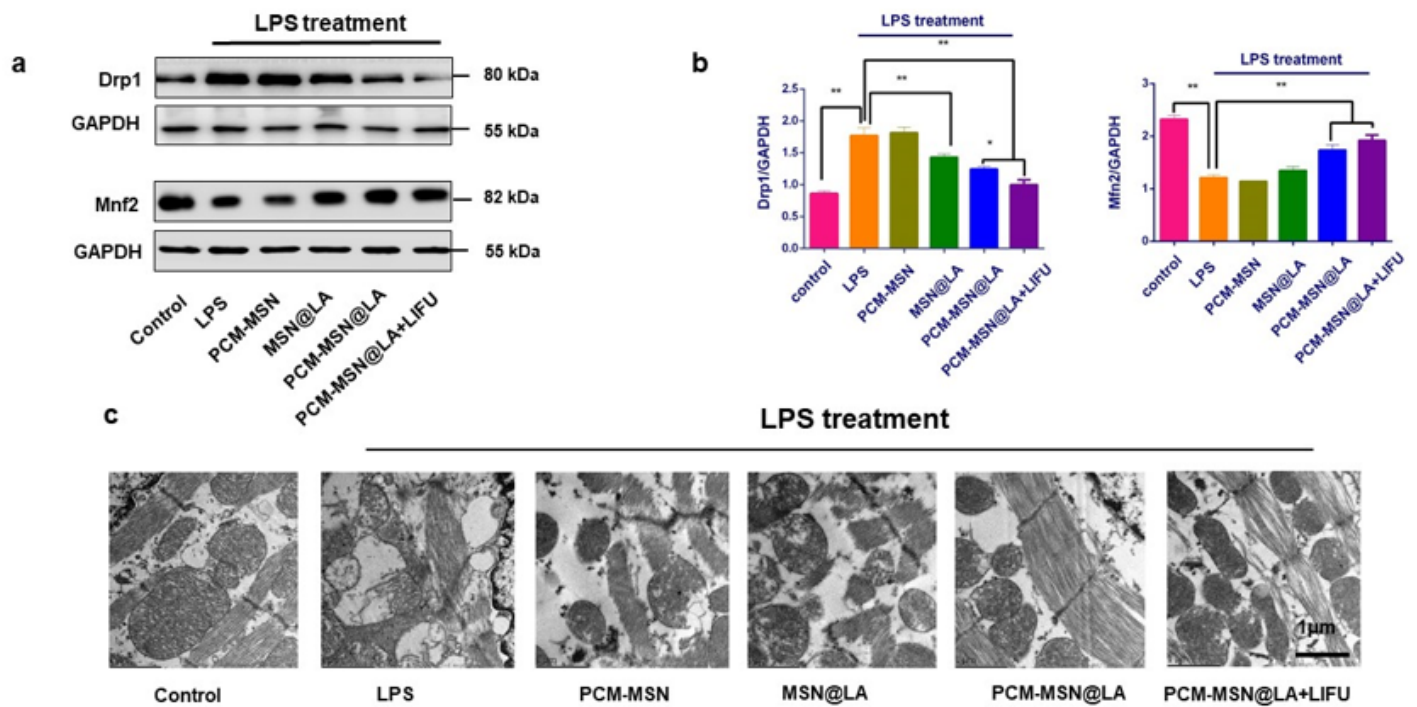
Figure 12

Myocardium-targeted NO release effectively protect LPS-induced myocardial mitochondrial dysfunction. a The expression mitochondrial mediator proteins Drp1 and Mfn2. b The quantitative analysis of Drp1and Mfn2 expression (n=8 per group; Data are presented as Mean±SD. *P<0.05 ; **P<0.01). c Electron micrographs of myocardium sections (n=8 per group; scale bar=1μm).

Supplementary Files

This is a list of supplementary files associated with this preprint. Click to download.

- Supplementary.jpg